TÉCNICO LISBOA

Application of dynamic rating to improve transportation capability of the power systems connected to Wind Power Plants.

Marco Merante

Thesis to obtain the Master of Science Degree in

MEGE

Coordinators: Marcellino Ferreira, Kateryna Morozka

Examination Committee

Chairperson: Prof. Duarte Sousa

Supervisor: Prof. Marcelino Ferreira

Members of the Committee: Prof. Ferreira de Jesus

September 2016

Abstract

Current flow in the electrical grid is changing due to the introduction of new generators and loads. Specifically, weak Overhead lines, are a constraint for the introduction of wind farms located far from the central network. The current situation requires smart solutions to improve the transportation capabilities of these grid's components. Among the different possibilities, Dynamic Line Rating (DLR), is emerging as the most interesting solution from both the economic and technical points of view. The presented Thesis work investigates the performance of DLR from both the theoretical and practical perspectives.

The theory behind DLR is based on the development of a thermal model able to estimate the precise temperature experienced by OHLs conductor under different climate conditions. Since 1972, when the first investigation on DLR have been published, different thermal models have been developed, each with a different precision level. The first part of the thesis concerns the investigation of IEEE 738 standard accuracy.

The standard analysis highlighted weaknesses on the theoretical approach employed on the forced convective cooling calculation. Specifically the wind direction effect is estimated as the conductor was a perfect cylinder. A wind tunnel test has been performed in order to verify the effect of the conductor's strands on the total thermal equilibrium.

The results show that an inclined wind-conductor relative direction can have a more important impact on the line rating than foreseen with the IEEE thermal model. Since the wind tunnel test has been the first experience of this kind pursued at KTH, the presence of few different laboratory set-up deficiencies did not allow to draw a definitive and precise conclusion on the necessary IEEE formula correction.

The practical side of the Thesis project includes an extensive literature research on the different devices that can be employed for dynamic line rating and a real-case study analysis. The analysis is performed in order to evaluate which can be the best solution when the introduction of new wind energy supply increase the load on a pre-existent OHL. Results show that, in the selected region, Värmland, in the southwestern Sweden, DLR has the prerequisites to allow the exploitation of the high wind energy resource at the lower expenses. Wind energy production is often associated with an increased cooling on the line's conductors. This means that higher current levels can be withstood avoiding the need for expensive lines' upgrading. For the selected hot-spot, in 2015, DLR would have allowed a transport capability improvement of 69.6% during the summer and of 26.7% during the winter. It is also reported that a load equal to the SLR during the winter period would have caused serious overheating transients of the conductor. Overall DLR proved to allow technical and economic benefit for the system operator.

Keywords: *Dynamic line rating, overhead lines, conductor temperature model, wind energy.*

Resumo

Na actualidade, as redes de transmissão e distribuição estão a enfrentar grandes desafios. As alterações dos perfis da produção e consumo de energia requerem uma maior flexibilização no despacho da energia ao longo da rede. Entre outras possibilidades, a classificação dinâmica das linhas de transporte de energia ("DLR - Dynamic Line Rating") emerge como a solução mais interessante tanto do ponto de vista económico como do ponto de vista técnico. Com a presente dissertação investiga-se o desempenho do DLR do ponto de vista teórico e na perspectiva da respectiva implementação.

A teoria que suporta o DLR baseia-se no desenvolvimento de um modelo térmico que permita estimar de forma precisa a temperatura dos condutores das linhas aéreas para diferentes condições climatéricas. Desde 1972, altura em que foi publicada a investigação pioneira em DLR, diferentes modelos térmicos têm sido desenvolvidos, cada um dos quais com diferentes níveis de precisão. A primeira parte da dissertação é dedicada à investigação da precisão da Norma IEEE 738.

A análise da Norma permitiu identificar como um dos pontos fracos da mesma a abordagem teórica ao cálculo da transmissão de calor por convecção forçada., especialmente no caso em que o efeito da direcção do vento é analisado como se o condutor fosse um cilindro perfeito. Um ensaio num túnel de vento foi realizado de forma a verificar-se o efeito dos fios do condutor no equilíbrio térmico global.

Os resultados mostraram que uma inclinação na direcção relativa vento-condutor pode ter um impacto mais importante na classificação da linha comparativamente ao modelo térmico da Norma IEEE 738. Dado que o ensaio no túnel de vento foi o primeiro deste tipo efectuado no KTH, as limitações do equipamento existentes não permitiram tirar conclusões definitivas e precisas sobre as correcções a introduzir nas fórmulas da Norma IEEE.

Do ponto de vista experimental, esta dissertação inclui uma extensiva revisão da literatura sobre os diversos equipamentos que podem ser utilizados na classificação dinâmica das linhas e uma análise a um caso de estudo real. A análise é realizada de forma a avaliar qual a melhor solução quando um novo gerador eólico é introduzido aumento a carga numa linha aérea pré-existente. Os resultados mostram, para a região de Värmland seleccionada (sudeste da Suécia), que a DLR satisfaz os pré-requisitos para permitir a exploração dos recursos eólicos a baixo custo. A produção de energia eólica está por vezes associada à necessidade de arrefecimento dos condutores das linhas. Isto significa que correntes elevadas podem ser suportadas evitando a necessidade the linhas sobredimensionadas e mais onerosas. Para o caso seleccionado, em 2015, o DLR teria permitido um aumento da capacidade de transporte de 69.6% durante o Verão e de 26.7% durante o Inverno. È também referido que uma carga igual à SLR durante o período de Inverno, poderia ter causado aquecimentos transitórios danosos no condutor. Na generalidade, a DLR mostrou-se como a solução mais interessante tanto do ponto de vista técnico como do ponto de vista económico.

Palavras-chave: *Classificação de linhas dinâmica, Linhas aéreas, Modelo térmico de um condutor, Energia eólica.*

Table of Contents

APPENDICES

Appendix A Excel and Matlab Model inputs.

Appendix B Matlab script. Solar heat flux calculation.

List of Figures

List of Tables

Nomenclature

AC	Alternating Current
ACSR	Aluminum Conductor Steel Reinforced
CF	Cash Flow
CFD	Computation Fluid Dynamic
CIGRE	Conseil International des Grands Réseaux Électriques
DC	Direct Current
DLR	Dynamic Line Rating
DPP	Discounted Pay-back Period
DSO	Distribution System Operator
EMS	Energy Management System
ENTSOE	European Network of Transmission System Operators for Electricity
EVDO	Evolution Data Optimized
IEEE	Institute of Electrical and Electronics Engineers
IRR	Internal Rate of Return
GMT	Greenwich Mean Time
GSM	Global System for Mobile Communications
OHL	Over-Head Line
PD	Power Donut
PMU	Phase Monitor Unit
PSG&G	Public Service Enterprise Group
PV	Photovoltaic
RTE	Réseau de transport d'électricité
SCADA	Supervisory Control and Data Acquisition
SMHI	Sveriges Meteorologiska och Hydrologiska Institut
SLR	Static Line Rating
TRM	Thermal Rate Monitor
TSO	Transmission System Operator
WACC	Weighted Average Cost of Capital
WMO	World Meteorological Organization

1. Introduction

Transmission and distribution networks are facing major challenges. The change in electricity production and consumption patterns requires more flexibility in the dispatch of energy through the grid.

Energy has been traditionally supplied by big power stations able to adjust outputs in order to follow the peculiar dynamicity of the demand (e.g. Hydropower, Nuclear, Carbon or oil thermal power plants). Under this assumption, the network has been shaped with the objective to dispatch constant forecastable power flows.

The conditions above underlined are not more valid since the renewable energy production share is rising year by year in order to decrease the human impact in the ecosystem.

Renewable energy production is characterized essentially by two factors:

- Distribution of the plants over a wide area in order to exploit the maximum available diffuse resource;
- Intermittent production due to the impossibility to precisely foresee the resource availability in time and space.

These peculiarities affect substantially the management of energy flows in the grid. Production peaks due to unexpected favorable weather conditions have to be handled carefully in order to ensure grid safety and reliability. If the supplied “green” energy will not reach the consumers in a safe and economical way the renewable production will remain pointless.

Under these conditions grid owners are struggling in order to face this radical change ensuring minimum expenses in network investments.

In order to avoid grid bottleneck and downtime losses for renewable plants (e.g. Wind farm) transport capability of weak lines in the network should be upgraded.

Among the different possibilities Dynamic Line Rating (DLR) is emerging as the most interesting solution from both the economical and technical points of view.

Up to now the ampacity of grid components have been estimated under conservative assumptions. The worst scenario is considered as the reference for the selected period. This means high temperature, low wind speed and solar irradiation on the line. This traditional rating approach is called Static Line Rating (SLR)

Real data collected in different lines shows that real-time climatic conditions allow higher ampacities respect the SLR scenario, especially in a country like Sweden where temperatures are in average mild and the wind flow quite constantly.

The work is divided in five different parts.

The **Introduction** gives an overview of the theoretical knowledge behind the DLR approach. It is necessary to understand why it is important to rate an OHL and how the rate (ampacity) is calculated.

Chapter 3 reviews the performed laboratory test. A wind tunnel have been employed to obtain precise measurement on the cooling process of an OHL conductor. The results have been compared with the IEEE thermal model predictions in order to verify if the effect of different wind speed angles is precisely obtained with the cited calculation standard.

Chapter 4 contains a literature research on the several devices available on the market for OHL monitoring and DLR calculation. These are then compared with alternative upgrading solutions; technically and lastly ethically.

Chapter 5 reports the performed investigation done on a real study case proposed by the Thesis company partner, Ellevio AB. The favorable wind conditions present in the Southwestern part of Sweden welcomed the installation of several wind farms. New turbines will be erected in the coming future and it is necessary to understand if the current energy grid is ready to accommodate higher energy fluxes due to the wind energy production. The study case concern specifically two OHLs and the installation of a new 27 MW wind farm. A technical and economic investigation is performed in order to understand what is the best adoptable solution for Ellevio AB.

Chapter 6 contains final reflections that conclude the Master Thesis project.

2. Background

2.1 History

The development of low-cost IT equipment in the 70' made DLR an interesting alternative for grids upgrading. The first article on the topic has been published in 1972 by Professor L. Fink [1].The cited paper describes the possible benefits of real-time monitoring of an underground transmission network.

Later on, around the end of the decade (1977) Prof. M.W. Davis investigated for the first time the same concept on overhead transmission lines [2]. The author conceived the idea on 1967 but only after a decade SCADA systems became prominent and it has been possible to test the concept on a real case analyzing real data from the Midwestern United States. His work pointed out how the probability to have, at the same time, low wind speed and high temperatures during maximum load levels in the reported area was negligible.

The conclusion was that SLR circumstances were pessimistic almost along all the length of the measurements period.

After the studies in the '70s, a real DLR monitoring system has been shaped and applied on transmission cables at Boston Edison in the mid 1980s. The system's name was UPRATE [1].

In 1989 real-time rating has been applied also on a transformer bank at LILCO (Long Island Lighting Company).

For what concern overhead lines more than a decade passed between Prof. M.W. Davis studies and the application in the industry world. In 1991 Nitech commercialized the firsts Power-Donuts. Power-Donuts (PD) measures directly the temperature of the conductor. These sensors coupled with USi's (the company that now commercialize PD3, third version of the mentioned equipment) real-time dynamic rating software and hardware provided the first DLR system for overhead lines [3]. This instrumentation package for real-time measurements allowed the development of a complete real-time monitoring and dynamic rating system for substation equipment, including switches, line traps, and bus. In 1999 already more than 1000 Power-Donuts were installed worldwide [3].

2.2 Consequences of conductor overheating

Restrictions in lines' ampacity are imposed in order to avoid issues due to conductors' overheating. An excessive temperature causes premature aging and possible dangerous sag levels of the line. In this chapter these two different issues are analyzed.

Annealing

Annealing is the main cause of the aging process of a conductor; it causes loss of tensile strength. When enough time passes, it can become the reason for outages and blackouts[4]. Annealing is one of the main sources of permanent damage of aluminum strands. For the mentioned metal, the following empirical formula shows how the loss is proportional to the temperature of the conductor:

$$L_{Al} = 100 - kt^{-\frac{1.6}{0.63d}(0.001 \cdot T_c - 0.095)} \qquad (1)$$

Where, L_{Al} is the percentage of loss of strength, d is the strand diameter [mm], t is the exposure time [hr], T_c is the conductor temperature [°C], and $k = -0.24 \cdot T_c + 135$.

Precisely aluminum annealing begins at 100 [°C] and become drastic over 200 [°C] [5].

In [4] the tensile loss of aluminum strands and of the compound conductor are calculated in a 5 years period. The nominal current of the line is 1000 [A]. Results are obtained for values 10, 20 and 30% higher respect the nominal current. Calculations are performed following the guidelines found in [6].

The results are reported in the following table:

Table 1: Tensile strength losses for aluminum strands and compound conductors under different current levels [4].

Current [A]	Loss of tensile strength [%]	
	Aluminum strands	compound conductor
1221	4.79	2.644
1332	9.987	5.513
1443	15.613	8.62

The emissivity measures of the conductor's surface (Aluminum Conductor Steel Reinforced) gives indications on the aging of an ACSR (Aluminum Conductor Steel Reinforced). The following empirical formula relates emissivity and age of a conductor [7].

$$\varepsilon = 0.23 + 0.7\,\frac{Y}{(1.22+Y)} \qquad (2)$$

Where Ɛ is the emissivity and Y the number of years the conductor has been energized. It can be noticed that when the conductor becomes older the emissivity increases. Typically, when the conductor is new, the emissivity is around 0.23[8]. in [6], after 5 years, the measured Ɛ is 0.793.

Line-to-ground clearance limits [9]

It is essential to control the sag of conductors along the spans of transmission or distribution lines. Sag is defined as the vertical distance between the point where the line is linked to the tower and the lowest point that the conductor reaches. Line-to-ground clearance is the distance between the lowest point and the ground. Between two towers the conductor will necessary bend. Line cannot be placed straight since low temperatures can contract the conductor causing over-tensions that will irreversibly damage the system.

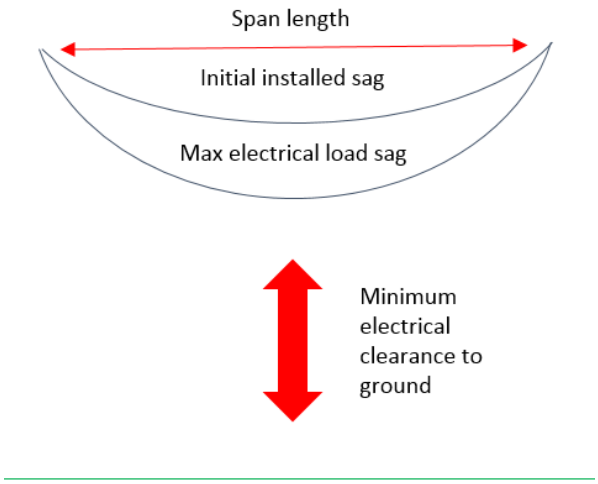

Figure 1: Illustration of sag in different conditions.

The bending shape of the conductor must be restrained to ensure public safety. High bending values can also possibly incur in power failures because the line can touch the ground or another conductor causing short circuits. Figure 1 gives a visual explanation of the different sags' values present in different conditions.

Sag can increase because of weather (ice, snow or wind) or load conditions. Specifically the latter is due to the increase of the conductors' temperature when the line current is high. In [10] conductor temperature and sag dependence is evaluated from real measures taken from a Swedish 130 kV transmission line (ZL8) on April 2011.

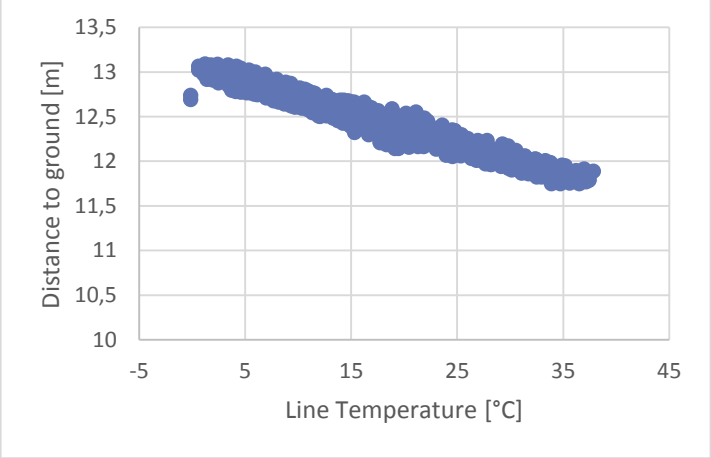

Figure 2: Measured distance to ground versus line temperature for April 2011, ZL8 [10].

The results in Figure 2 shows that there is a linear relationship between the evaluated variables (valid for the selected span), temperature and sag. Precisely the following linear regression has been obtained:

$$Z = -0.037\,Tc + 13.11 \qquad (3)$$

Where Z is the distance to ground [m] and Tc the conductor temperature [°C]. This means that for each Celsius degree conductor's temperature increase the line sags 3.7 cm more. This effect will be further evaluated along the project because of its crucial importance respect the objectives of DLR. To give an example the following table depicts the clearance to ground limits present in the National Electric Safety Code (NESC) developed by IEEE in 1990.

Table 2: Data from [Sag & Tension Data Table, NESC, IEEE 1990]. [11]

Voltage Level	Clearance to Ground
less than 66 kV	6.1 m
66 to 110 kV	6.4 m
110 to 165 kV	6.7 m
more than 165 kV	7 m

Precisely the Swedish standard ELSÄK-FS 2008:1[12] reports that the minimum clearance to ground for OHL with a voltage level major than 55 kV have to be 7+S in case of detailed planned area and 6+S in case of not detailed planned area. S is an addend that depends on the OHL voltage level. S values are reported in the following table:

Table 3: Voltage dependent addend (S) for OHLs in Sweden. [12]

System voltage kV Voltage dependent addition (S)	Directly earthed system	Non-directly-earthed system
77		0.2
132	0.4	
220	0.8	
400	1.7	

2.3 OH lines thermal models

Ampacity depends on the conductor temperature. The equilibrium temperature value can be calculated in steady state conditions from the following thermal balance:

Heat Losses = Heat Gain

Starting from this equivalence mainly two methods have been developed and adopted to analyze the thermal heat balance of an OH conductor, one developed by IEEE and the other from CIGRE.

CIGRE formula [13]:

$$P_J + P_M + P_S + P_i = P_C + P_r + P_w \quad (4)$$

IEEE formula [8]:

$$P_J + P_S = P_C + P_r \quad (5)$$

Where:

P_J	Joule heating (due to current flow);
P_M	Magnetic heating;
P_S	Solar heating;
P_i	Corona heating;
P_C	Convective cooling;
P_r	Radiative cooling;
P_w	Evaporative cooling.

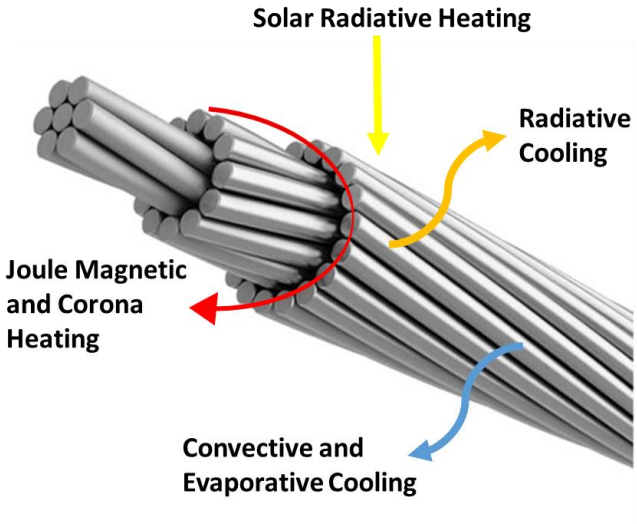

Figure 3: Heat fluxes representation.

Different articles comparing the two methods outcomes can be found in the literature. Some says that results are practically the same, Schimdt [14], and other that normally the difference is around 5-15% [15]. The respective formula components will be analyzed to understand where differences create discrepancy.

The first point that can be observed is that CIGRE formula includes three terms more than the IEEE one: P_M, P_i and P_w. Corona heating, P_i, is the result of the air dissociation in ions due to voltages higher than the dielectric disruption value (30 kV for air). The process creates light and heat but has practically no influence on ampacity calculations [15]. Magnetic heating is due to Eddy currents, hysteresis and magnetic viscosity; phenomena caused from the cyclic magnetic flux created by the AC current flowing in the conductor. Magnetic heating is present as a separated term by CIGRE and included indirectly by the IEEE approach since the latter instead of using the DC resistance for joule heating calculations employs directly the AC resistance value [13].

Evaporative cooling does not affect significantly the heat transfer process in absence of precipitations. It has a critical role only when the conductor is completely wetted (rain). In general this effect is mostly ignored [15].

The remaining terms are common but calculated with different methods.

Solar radiation, P_S, is obtained starting from different parameters in the IEEE and CIGRE cases.

IEEE [8]:	CIGRE[13]:
- Sun Altitude	- Direct radiation
- Sun Azimuth	- Diffuse radiation
- Heat flux received by a surface at sea level	- Reflected radiation

IEEE calculates only direct radiation from the considered values and this make the method easy but the results less precise. The use of CIGRE approach results in higher expenses due to the high cost of radiation meters. Generally, CIGRE method results in 10-15% higher values in respect to IEEE approach [15].

Convective cooling includes natural and forced contribution in both cases.

IEEE [15] separate between high (qc1) and low (qc2) wind speed situations for forced convective cooling:

$$q_{c1} = \left[1.01 + 0.0372\left(\frac{D\rho_f v_w}{\mu_f}\right)^{0.52}\right] K_f K_{angle}(T_c - T_a) \qquad (6)$$

$$q_{c2} = \left[1.0119\left(\frac{D\rho_f v_w}{\mu_f}\right)^{0.6}\right] K_f K_{angle}(T_c - T_a) \qquad (7)$$

Where:

- q_{c1}, q_{c2} Convection heat loss rate;
- ρ_f Density of air;
- v_w Speed of air stream on the conductor;
- K_f Thermal conductivity of air;
- μ_f Air viscosity;
- T_c Conductor temperature;
- T_a Ambient air temperature.

The range of application of the two formula is not well defined. Wrong estimations can result in important errors. IEEE adopts a conservative solution, to obtain both results and consider the bigger one.

It can be noticed that the two formula include K_{angle}. It is defined as:

$$K_{angle} = 1.194 - cos\theta + 0.194cos2\theta + 0.368sin2\theta \qquad (8)$$

Where θ is the angle between the wind direction and the axis of the conductor. This factor take in account the different effect the wind direction has on forced convective cooling. This coefficient is obtained from the studies conducted by Prof McAdams around the half of the past century [16].

He performed wind tunnel tests on a cylinder. This factor will be better analyzed in chapter 3 since its calculation and effect are the ones that will be compared with the laboratory results.

Natural cooling contribution is obtained from:

$$q_{cn} = 0.0205\rho_f^{0.5} D^{0.75}(T_c - T_a)^{1.25} \qquad (9)$$

CIGRE [13] approach is more theoretical and take in account Nusselts, Reynolds, Grashof and Prandtl non-dimensional numbers. If these values can be obtained precisely the physical cooling process can be accurately calculated through the following formula:

$$P_c = \pi\lambda_f(T_s - T_a)Nu \qquad (10)$$

Where:

- **λf** Thermal conductivity of air;
- **Nu** Nusselt Number;
- T_s Surface temperature;
- T_a Ambient air temperature.

It can be noticed that CIGRE standard considers the conductor surface temperature while the IEEE temperature value is considered constant along the length of the conductor radius. The Nusselts number, that express the ratio between the conductive and convective heat flux, is calculated as:

$$Nu = B_1 Re^n \qquad (11)$$

Where:

- **Re** Reynolds number;
- **B1** and **n** Constants that depend on the conductor kind.

CIGRE approach consider, through the selection of the different constants B1 and n, the not uniform surface of the OHL. B1 and n in fact depend on the conductor surface roughness R_f:

$$R_f = \frac{d}{2\,(D-d)} \qquad (12)$$

Where d is the diameter of the strands and D the total of the conductor.

The direction of the wind is taken in account modifying Nu:

$$Nu_\delta = Nu_{90°}[A_1 + B_2(sin\delta^{m1})] \qquad (13)$$

Where:

- $\mathbf{A_1}$ = 0.42, $\mathbf{B_2}$=0.68 and **m1** = 1.08 for 0° < σ < 24°
- $\mathbf{A_1}$ = 0.42, $\mathbf{B_2}$=0.58 and **m1** = 0.90 for 24° < σ < 90°

For low wind speed the direction does not influence the convective cooling and the Nu is reduced by:

$$Nu_{cor} = 0.55Nu_{90°} \qquad (14)$$

Cooling by radiation is obtained in the same way [8], [13] from the following expression:

$$P_r = \pi D \varepsilon \sigma_B [(T_s + 273)^4 - (T_a + 273)^4] \qquad (15)$$

Where the emissivity **ε** is dependent on the conductor surface and varies from 0.27 for new stranded conductors to 0.95 for industrial weathered conductors, σ_B is the Stefan-Boltzmann constant, T_a is the ambient temperature and T_s is the conductor surface temperature[8].

IEEE and CIGRE standards are both effective and provide satisfying results. In average they vary between each other by no more than 5-15%. This similarity has been achieved in 2007, when IEEE updated the standard and adopted more universal calculations (instead of only tabulated data). In general it is not possible to say which method is better since each situation is different and it always depends on which data are available. CIGRE standard is generally more complex and include different details but it has to be considered that some cases can be estimated with enough accuracy without taking in account to many details.

2.4 DLR Models

The heat transfer process of a conductor can be modelled starting from different parameters in different ways. The objective is to achieve the tradeoff between precision and system costs. Several arrangements can meet the objective basing on the different situations where DLR has to be applied. The following chapter will review the proven configurations.

OHL parameters can be monitored in real time by different devices connected to the operational center in different ways. The important line's characteristics are tension, sag and temperature. Line rating can be calculated by computer programs if line's load and weather conditions are also known [17].

Line ratings cannot be calculated from a singular input. To rate means to have an understanding of how the component behaves basing on the different conditions it will experience. This means that different parameters should be evaluated and crossed-checked to obtain a reliable forecast on the line behavior under different weather conditions.

The first software that has been developed to elaborate different measurement inputs and obtain the rating of grid component's is EPRIS's DTCR(Dynamic Thermal Circuit Rating) [18].

This software contains three different models for calculations. These models represent a classification of all the different set-ups that have been employed and are still used nowadays. These are:

- Weather Based DLR
- Temperature Based DLR
- Sag/Tension Based DLR

Weather- Based DLR

The weather-based method estimates the rating from weather and load data. Through one of the heat balance of the conductor as shown in chapter 2.3 it is possible to calculate the conductor temperature and therefore rate the OHL.

It represents the simplest and cheapest approach since no devices have to be installed directly on the line and survive a high electromagnetic environment [18]. The accuracy of the method depends on the number and proximity of weather stations to the OH line [17]. The higher the number and the closer to the line, the better will be the temperature estimation. The measured data have to be the closer possible to the ones experienced by the conductor itself.

The main advantages of this method are [18]:

1. Independency from line current;

2. The monitoring equipment is relatively cheap, not requiring line outages to install and expensive maintenance operations;

3. Weather data may also be used to rate all the close grid equipment.

The disadvantages are that the anemometers are quite fragile and imprecise and that many different weather station could be necessary for long lines in various terrain conditions.

Temperature based DLR

Through this approach the rating is obtained starting from a direct measurement of the conductor temperature in combination with the line current, air temperature and solar heating values [17]. The update conductor temperature is converted to an equivalent wind speed perpendicular to the line. Then knowing all the weather parameters, the rating can subsequently be obtained through the same heat balance equation used in the weather-based approach. This method as the advantage that a direct measurement of the temperature is available. In this way a fast feedback of the line conditions is available.

The temperature is normally measured by devices placed directly on the conductor. Another approach to estimate the conductor temperature is through PMU (Phase Measurement Units) as it is analyzed in [19], [20]. If a linear relationship between resistance and temperature of the conductor is accepted, obtaining the resistance value through electrical data analysis will make the conductor temperature available. PMU installations are growing in many countries' grid and this means that the method can be implemented without additional costs since no extra devices need to be installed on the line. In addition, the calculated temperature, is related to the average along the line and it is not affected by local microclimates and the radial temperature profile. This method still need improvements to increase the accuracy of the results.

Sag/Tension based DLR

The majority of transmission and distribution lines are constrained by clearance to ground limits and not by annealing issues [18]. In these cases a direct determination of the sag amplitude is important. Sag is directly related to the line tension. Line's tension magnitude depends on the average weather conditions present along all the spans between two tension poles. The consequence is that ratings based on a single sag-tension monitor are comparable with ratings obtained through several weather stations along all the line sections. Tension monitors are

normally installed when the line is de-energized. This means that commonly to apply this devices an outage is required.

The ampacity is obtained as in the temperature based model. The tension is converted to its equivalent wind speed [17] in two steps. Firstly the tension is converted to the average line temperature from the tension-temperature relation previously obtained from the calibration process. Secondly, as for the temperature based model, the temperature is converted to the equivalent average wind speed along the line section. From the heat balance equation the line rating is obtained.

None of these methods is generally better than the others. Line conditions and rating situations can vary on a large scale and for each different case a certain method can constitute the optimum choice. The utilization of the different approaches also depend on the market available devices. DLR state of the art equipment will be analyzed in chapter 4.

3. Experiment

3.1 Experiment objectives

Since two decades the concept of dynamic line rating made the step between being just a theory and become actually used in the reality to increase the loadablity of power-grid lines. During this period many data have been collected from the transmission lines and from different laboratory tests. These analyses have been performed to predict *a priori* the beneficial impact accomplished by the use of DLR[21]–[25].

Precisely, considering the performed Lab tests as of now, it is possible to recognize how, in the different study cases, attention has been devoted mainly to wind speed cooling magnitude and radial temperature profile of the conductor. Few tests can be found concerning the verification of how different wind flow directions affect the heat transfer process.

The majority of DLR devices employ either the IEEE or CIGRE calculation standards[8] to obtain the rating from the measured parameters. The standards procedure have been described in chapter 2.3.

The laboratory tests aim specifically at the verification of the $\mathbf{K_{angle}}$ formula (present in the IEEE standard) that consider the wind flow direction effect. Being obtained for perfect cylinders, it is expected that the results will fit precisely the real case of an OHL conductor.

Specifically the hypothesis that support the investigation lays on the creation of a turbulent area around the conductor when it is impacted by an airflow. This should happen because of the roughness created by the particular shape of OH conductors. In fact, OHL conductors consist of a number of wire strands woven together in a carefully designed pattern. The not perfect circular external profile will incur in the creation of a turbulent layer all around the conductors and necessarily modify the convective cooling coefficient and thus the final heat transfer rate.

It is expected that decreasing the angle between line and wind direction the turbulent area will spread along the OH piece. This, if turbulence is taken as a mean to increase the heat transfer rate, will hypothetically increase the difference between practical and theoretical results.

It is difficult to foresee the final effect on the heat exchange rate since the turbulence that will be created in the boundary layers between aluminum and the air cannot be calculated trough easy arithmetic and requires generally the use of CFD software. It has been demonstrated that in closed heat exchangers' tubes, turbulence created as embedded vorticity has the ability to improve the convective heat transfer coefficient thanks to the effect on the Nusselt and Prantdl number [26], [27]. These kind of results however cannot be directly extrapolated and applied to the test case since the overhead line is placed in the air and the eddies created by the turbulent flow have the ability to expand in a larger area and cannot be controlled.

The experiment aims at increase the reliability of the DLR concept enriching the knowledge about the convective cooling of an OHL.

3.2 Background

Several experiments concerning DLR can be found in the literature. All of them used a different set-up respect the one selected for the performed laboratory. The following review will outline the main tests characterizations and outputs.

Between 1982 and 1991 different experiments have been performed on the outdoor research facilities of the General Electric High Voltage Laboratory in Pittsfield, Massachusetts (Figure 4). The same test loop has been built indoor and has been placed in front of different fans fixed in a 30° direction respect the conductor.

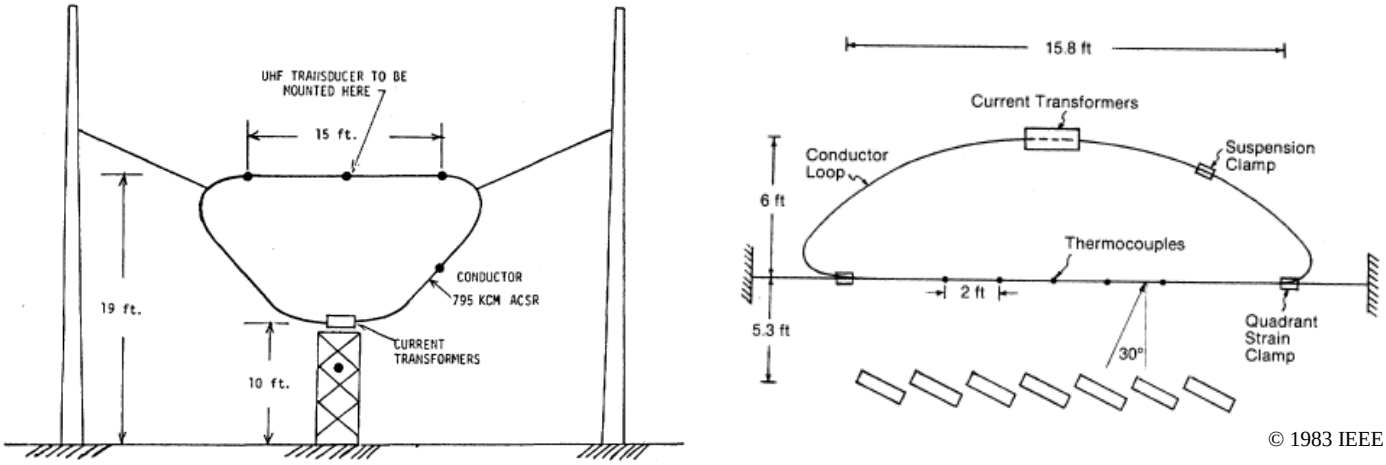

Figure 4: Laboratory Outdoor (left) and Indoor (right) Test Facility Conductor Test Loop. [73]

Current could have been regulated between 0 and 2000 A through the current transformer (Figure 4). This current level was enough to reach temperatures higher than 125 °C. Thermocouples have been placed in contact with both the surface and the steal core of the conductor.

The experiment goal was to compare field data test with thermal model [28] predictions. In addition the radial temperature profile have been analyzed to understand how thermal streams flow in a stranded conductor.

1983's experiments goal was to verify the prediction capability of the developed thermal model. Results showed an excellent agreement between field-test and Thermal model calculations.

Tests conducted in 1985 [29] substantiates the importance of the conductor temperature gradient monitoring. Conclusions states that the radial temperature difference under still air conditions is relatively insignificant compared to the magnitude of the conductor temperature rise over ambient (the radial temperature difference for a Drake 795 kcmil ACSR conductor represented approximately 5% of the conductors temperature rise over ambient). The relative significance of the radial temperature difference increases substantially as wind speeds exceed 1.79 m/s. With a wind speed of 1.79 m/s, the radial temperature difference for the Rail 954 kcmil ACSR conductor represented 40% of the conductors temperature rise over ambient.

It is important to notice that the different conductors have been tested with and without applied tensions. The results showed that internal temperature gradient decreased by approximately 40% when tension has been applied to previously non-tensioned conductors. Similar results have been obtained in [30] (10-20 °C core-surface temperature drop with tension and 20-40 °C when the conductor stands were slack).

Other results from 1991 are reported in [31]. Several indoor and outdoor experimental tests employing a Drake ACSR conductor have been performed to verify the original and a simplified thermal models mentioned in [31]. It has been found that, in comparison with the observed data, both model predictions are rather accurate even in the highly fluctuating outdoor environments (as it is showed in Figure 5). The result for an Indoor test is presented below.

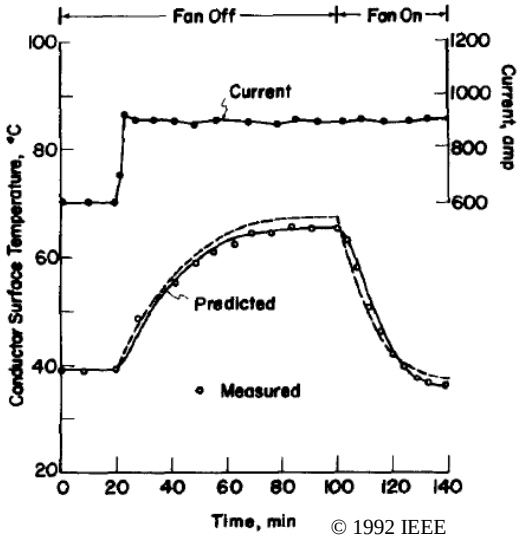

Figure 5: Conductor temperature response to current transient from 600 to 900 A of indoor test. (———) Predicted by the original model. (- - - - -) Predicted by the simplified model. [31]

A more recent experiment has been performed at Queen's University Belfast, in the UK [21].

Two set-ups have been tested. One in still air and the other enclosed in a wind tunnel. The different rigs have been used to examine the thermal behavior of the conductor under controlled environmental conditions with and without the forced convection. The analyzed conductor was an aluminum steel reinforced 'Lynx' 175 mm² conductor. The same conductor is used in a 110 kV Irish circuits were a significant amount of wind power is installed.

The conductor has been tested under two different step up currents; 0-250 A and 0-500 A. This has been done in steady air and different wind speeds (only on perpendicular direction). Temperature sensors have been placed on leeward, windward sides and on the core of the conductor.

The results for the wind tunnel 0-500A core temperature test are reported in the following Figure.

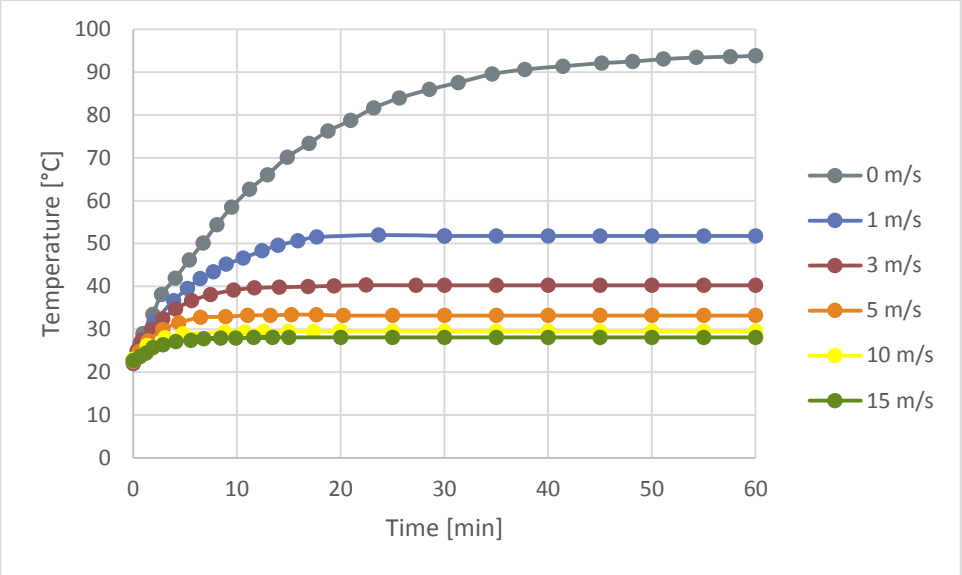

Figure 6: 0-500 A step up current heating under different wind speeds. [21]

44.6% of the total temperature reduction has been achieved in the first 1 m/s step. In this case, the temperature difference between windward and leeward sides has been 0.6 °C; this difference decreased sensibly with higher wind speeds.

3.3 Personal contribution

The Thesis project includes the participation in the laboratory test leaden by the Master Thesis supervisor, Kateryna Morozovska. The performed laboratory has been the first attempt to simulate OHLs cooling behavior at KTH.

The following contains a list of which have been the personal contributions for the laboratory set-up organization and execution:

- Literature research analysis on previous similar experiments;
- Laboratory objectives identification;
- Technical drawings of wind tunnel windows;
- Participation in components assembling;
- Participation in laboratory tests;
- Personal data results analysis.

3.4 Methodology

Equipment

One of the available wind tunnels of KTH aerodynamic department has been employed to simulate the cooling of different pieces of overhead lines under different wind flow conditions.

The following pictures shows the accessible wind tunnel section.

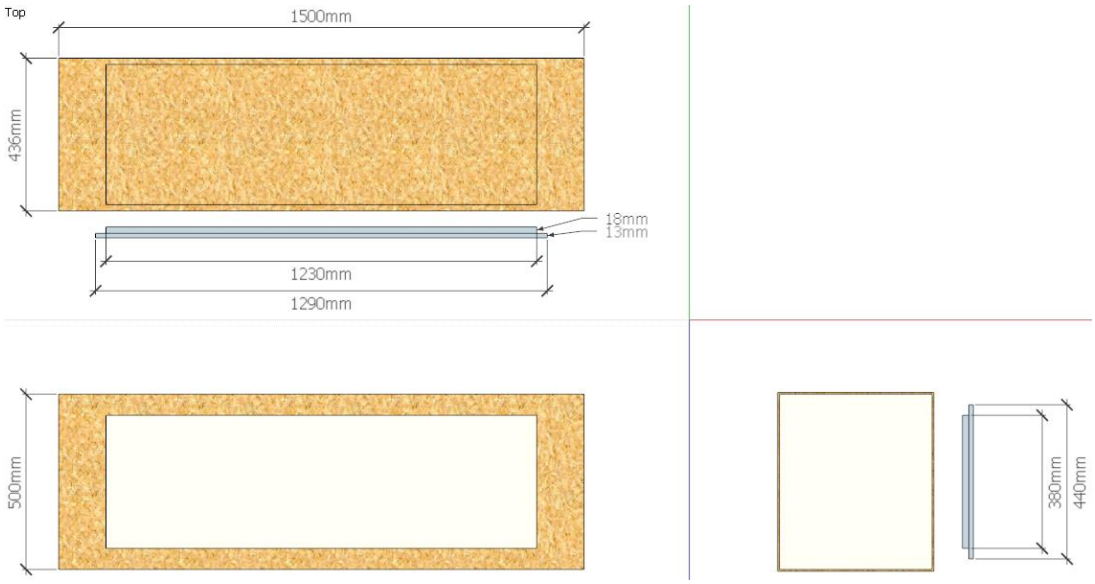

Figure 7: Technical drawing of the employed wind tunnel test section.

The tunnel section has four wooden windows on the left, right, top and bottom sides. The right and left windows have been replicated and modified. On the windows sections different circular holes have been drilled to host two conductive steal junctions.

The junctions are shaped in order to accommodate different conductors' diameter. Junctions are then fixed on different holes present in the windows in order to obtain measurement with different angular position. This configuration avoid the creation of air leakages on the windows. Leakages would disturb the air flow inside the wind tunnel section.

The wind is created through a fan placed downstream respect the accessible tunnel section. Wind speed can be adjusted, varying the fan rotation speed, between 0 and 25 m/s.

The Power have been supplied directly from the laboratory electrical grid. Since high currents are needed to simulate the real load of OHL a variable and a fixed output transformers have been placed in series. The high final transformer ratio allowed to reach currents up to 600 A. The current has been regulated manually changing the spires ratio of the autotransformer.

Sensors

The variables that have been measured are wind speed, current and conductor temperature:

- Wind tunnel speed has been regulated by changing the rotation speed of the fan. A Pitot tube has been employed to measure the wind speed in front of the conductor;
- The current has been measured through two current probes applied on the copper connecting cables;
- Temperature has been measured in different conductor's position through thermocouples (purchased from JUMO) applied in small drilled holes filled with thermal paste. The data logger has been purchased from Pico technology. Specifications are available in [32].

Temperatures have been monitored and saved through Pico software. Wind speed and current have been traced and analyzed employing National Instrument design software called LabVIEW [33].

Ellevio AB provided several OHL pieces to be tested. The following table lists the different conductors.

Table 4: Tested Conductors.

Code name	Nominal Area [mm²]	Stranding and Wire Diameter [mm]		Overall Diameter [mm]	Resistance [Ω/km]
		Al	Steel		
Ibis	234	26/3.14	7/2.44	19.9	0.1430
Dove	329	26/3.72	7/2.89	23.6	0.1020
Al 59	241	19/4.02	0	20.1	0.1230
Al 59	454	61/3.08	0	27.7	0.0654
Al 59	593	61/3.52	0	31.7	0.0501

The highlight yellow conductors are the one that have been tested in the 13 days long test.

The procedure consisted on heating up the pieces until the steady state temperature value. Once the equilibrium in steady air is achieved the fan is powered and the wind cooling process is traced until a new equilibrium temperature is reached. The new temperature allows to obtain the increase in the wind convective forced cooling. The procedure is then repeated for different wind speeds, conductors and angles.

In addition to the cited conductors an Aluminum rod has also been analyzed to compare its cooling process with the Al 59 241mm^2 conductor. The rod has same diameter and length.

Results have been subsequently compared with a developed thermal model in order to verify the initial hypothesis.

3.5 Thermal model comparison with other laboratories experiences

The transient heat transfer process has been modelled following the guidelines of IEEE standard [8]. The development tool of Excel is employed in this step to iteratively calculate how the conductor temperature change due to different external conditions. Joule heating, convective and radiative cooling are considered in this step. Solar heating is not considered since the tests have been conducted indoor. In order to validate the developed model, its outputs have been compared with results obtained in other Tests experiences

Figure 8 represents the results obtained by the previously cited UK laboratory [21] and the equivalent outputs of the developed model. A satisfying match is present for both temperatures ad time constants.

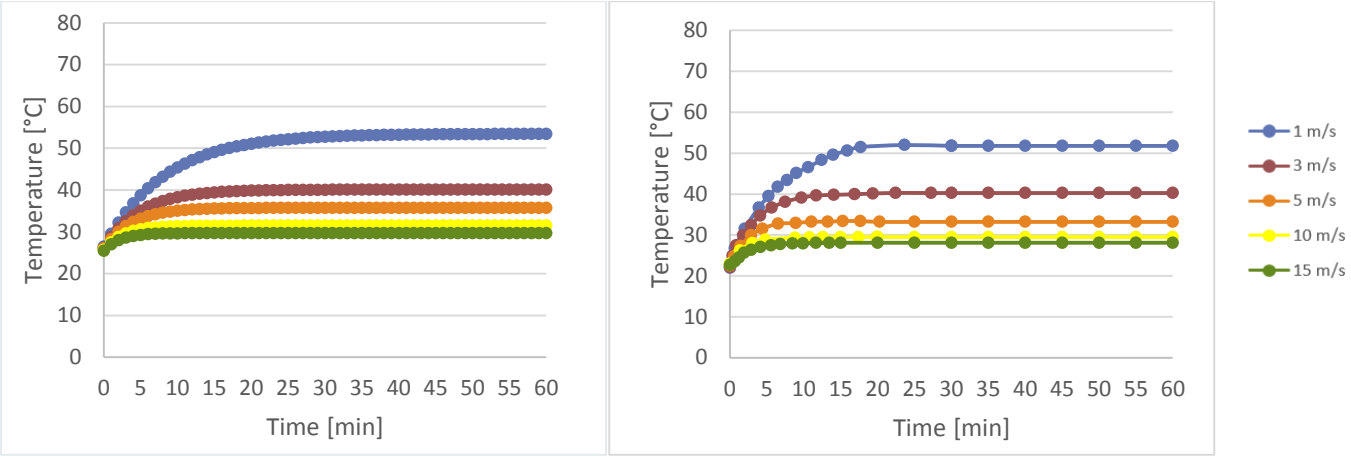

Figure 8: Developed IEEE Model (left), UK laboratory (right) comparison (LYNX 175 mm² conductor, 90°). [21]

An accurate correlation has also been found with results obtained by the IEEE 1985 indoor test. The results are showed in Figure 9.

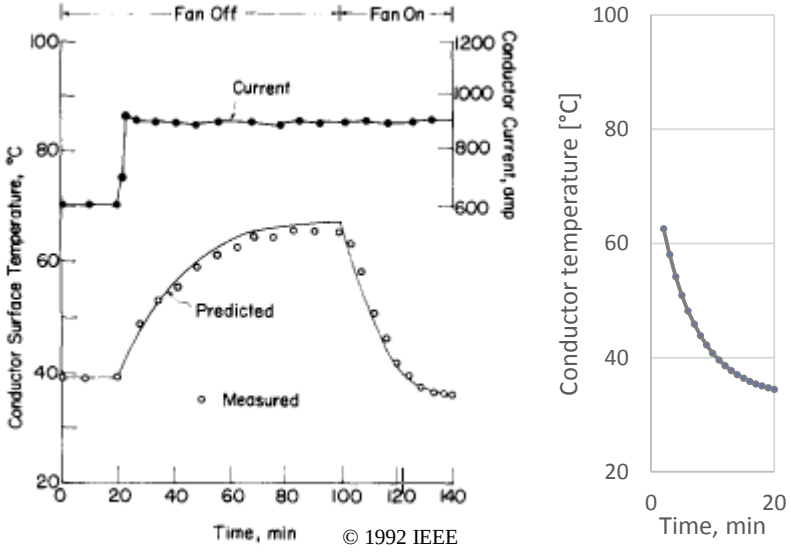

Figure 9: Conductor, Drake (Section 28,11 mm) , wind speed 1.83 m/s, angle 60°.

The resulted time constant has been around 6 minutes for both cases with a final temperature around 35 °C.

Thanks to this verification it is concluded that the developed model is reliable and can be employed to check the laboratory results.

3.6 Results and Discussion

The obtained results are presented and discussed. Laboratory measurements are analyzed to understand how the different variables affect the conductors cooling. The results are compared with the developed thermal model. The Excel model calculates the thermal transient of the OHLs pieces taking in consideration Joule heating and convective and irradiation cooling. Overall, the results show a not satisfactory match between laboratory and model results. The developed KTH laboratory set-up experienced higher temperature and thermal time constants respect the model forecasts. This could have been a consequence of the system high thermal inertia. This effect is most probably due to the short conductor pieces length compared to the heavy and substantial junctions' dimensions.

The following graphs report the results obtained for the Al59 241mm^2 conductor. The graphs show the comparison between two different wind angles (90° and 40°) for the test and model cases. The considered wind speeds are 1,2,5,10 and 16 m/s.

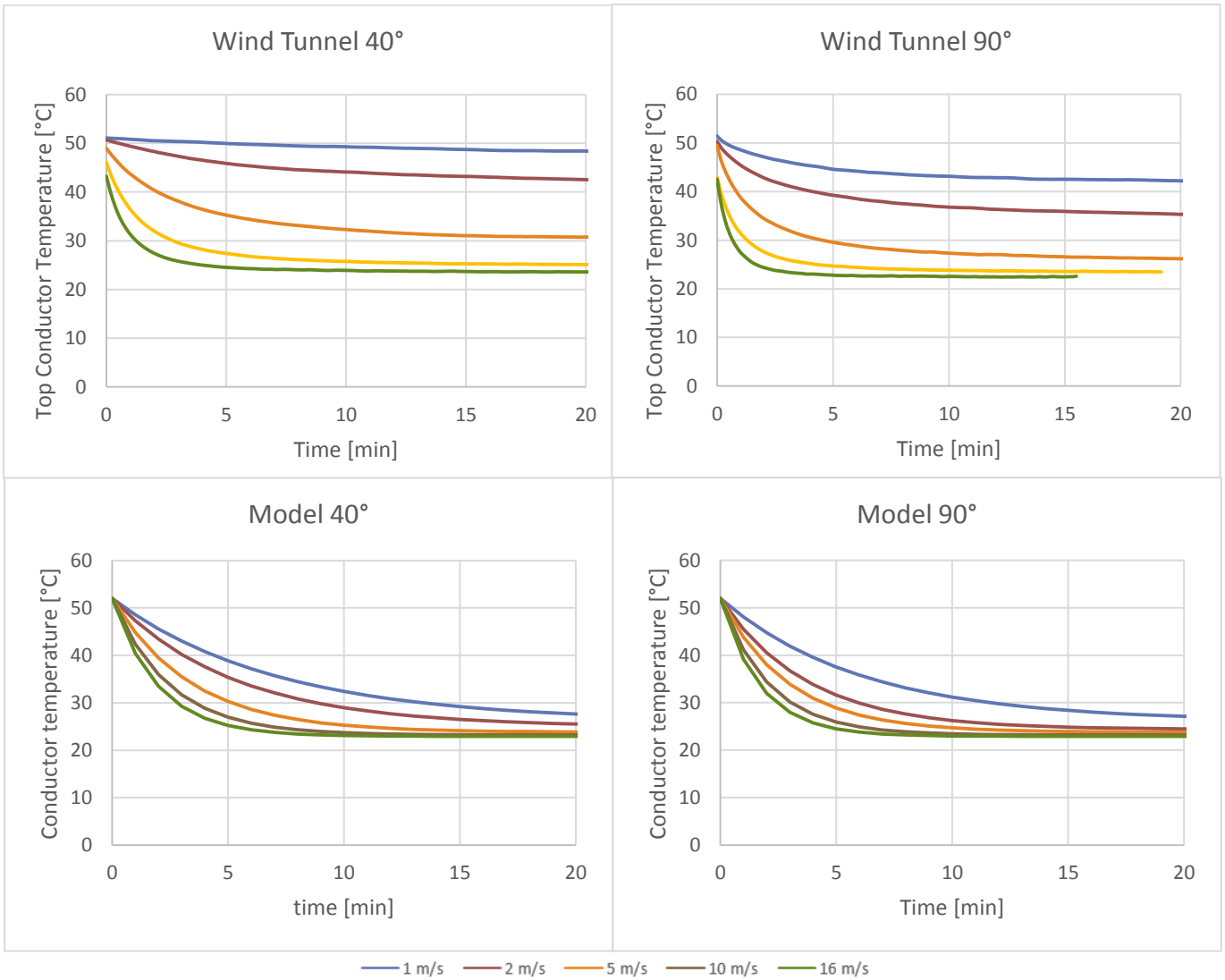

Figure 10: Al59 241mm^2 conductor test results. Comparison between different results for the following wind speed [m/s]: 1, 2, 5, 10 and 16.

In Figure 11 it is possible to notice the steady state temperature in the different considered cases.

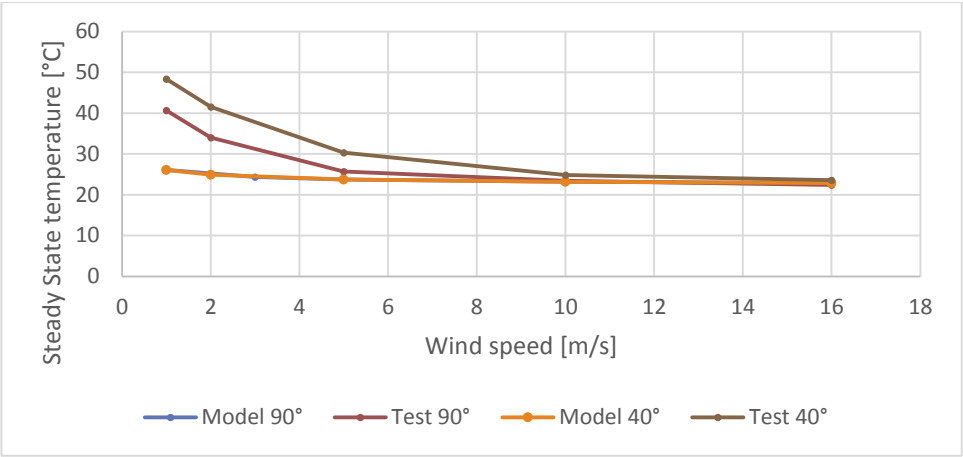

Figure 11: Final steady-state temperatures in the different analyzed cases.

The test equilibrium temperatures are higher for low wind speeds and became similar to the model ones for higher values. The steady state temperature for the 90°, 1 m/s case is 185% the value obtained from the model calculation for the same status. While it is possible to notice a substantial difference between the two different directions in the test results (22% higher for the inclined respect the perpendicular direction at 2 m/s), practically no differences are found in the model example.

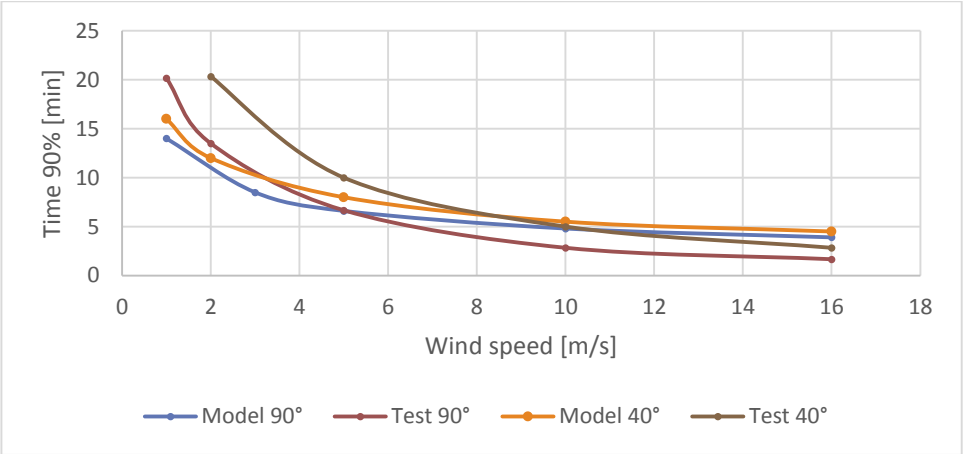

Figure 12: Comparison of the Time to reach 90% of the difference between start and steady state temperature.

Else than the final temperature it is important to understand how fast the conductor cools down when the wind conditions change. In the reality, if the wind speed increases, the wind farm output will grow at the same time. If a good correlation between OHL location and farm is present, the increase in the wind energy supply will be associated with an increase of the cooling rate of the conductor. These two phenomena will take place with different transitory, thus it is important to evaluate the time constant of the cooling process.

In the above graphs the time to reach 90% of the total temperature difference is reported. This value has been chosen because of the 10 seconds time step between two consecutive measures. For higher wind speeds, because of the fast cooling process, the time step did not allow to evaluate precisely a decrease of 62.3% defined as the standard time constant.

The measured periods during the tests have been longer respect the model outputs for low wind speeds and shorter for higher. In the 90° case the laboratory time constant passed from being 44% higher to 57 % shorter respect the thermal model foreseen results.

Regarding the difference between the two different conductor directions it is possible to notice that the discrepancy between the two sets of values has been greater in the laboratory case respect the model results(e.g. with a wind speed of 5 m/s the difference in the model is of 21% while the difference in the test is 50%).

3.7 Comparison with Aluminum Rod

An aluminum rod have been tested in order to further evaluate the effect of a stranded structure respect a perfect cylindrical conductor. Aluminum rod and conductor have the same diameter (20 mm).

It is possible to notice from the graphs in Figure 13 that discrepant results are found between the behavior of the two different conductors. Overall it is possible to notice how the final temperature profiles in the two cases are quite similar. On the contrary, the time to reach 90% of the total temperature range rises heavily for the rod case.

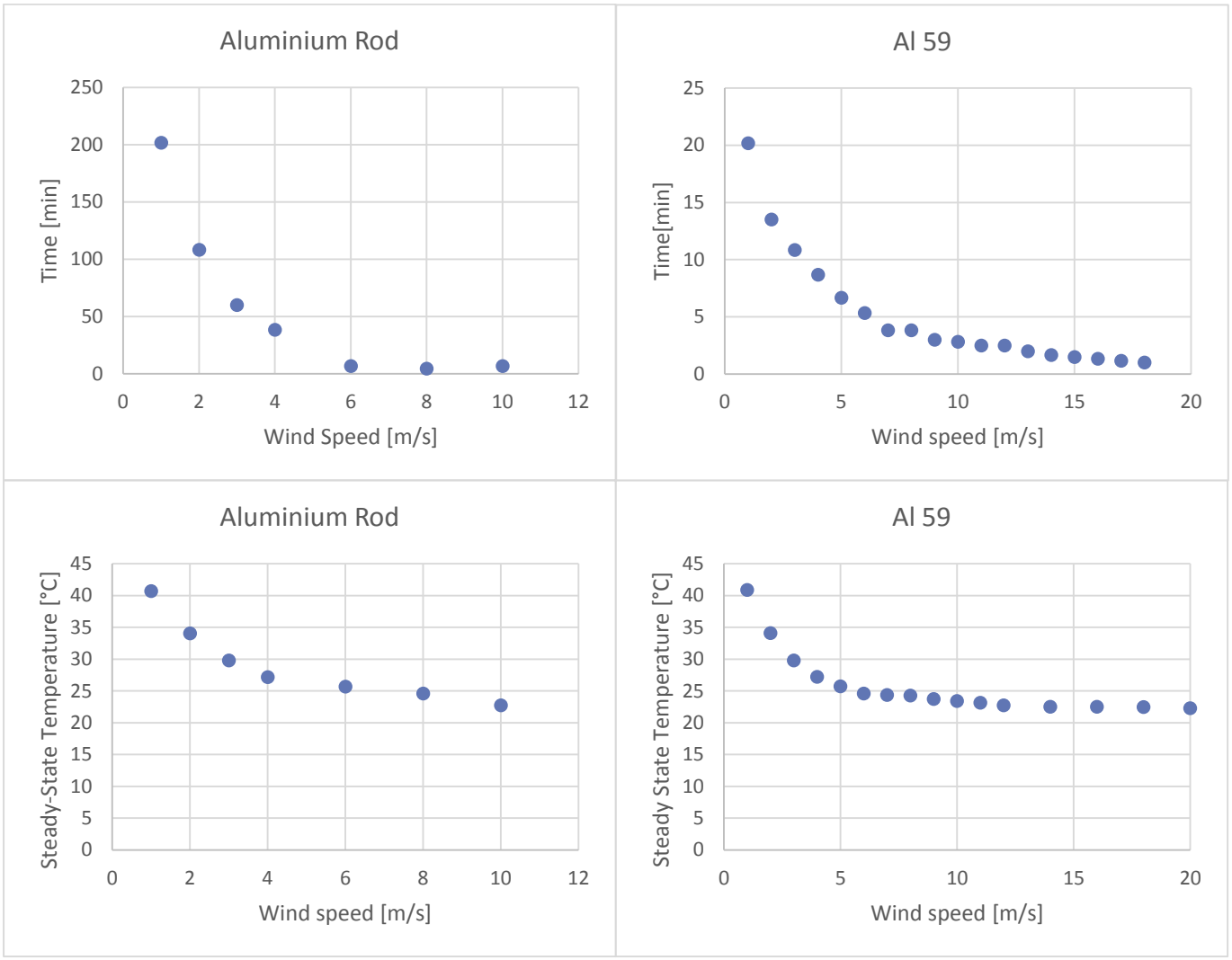

Figure 13: Results comparison between aluminum rod and same diameter dimension aluminum stranded conductor (for an average current of 230 A).

With a wind speed of 1 m/s the rod time constant have been 10 times higher respect the stranded conductor. Increasing the wind speed the difference in the cooling time decreases. In fact, with a wind flow of 8 m/s, the calculated time constant for the rod is of 4.5 minutes while for the conductor is 3.83 minutes (circa 20% higher).

It is showed that considering aluminum conductors as cylinders would bring to inexact results. For this reasons results obtained from the CFD simulation employed in [34] should be carefully evaluated.

CFD analysis has the potential to further analyze the thermal exchanges in OHL conductors. To obtain valuable results it is necessary to create fine meshes that replicate exactly the stranded structure of the conductor. If this is not fulfilled results will poorly emulate OHLs conditions affecting the reliability of the results.

Due to time constraints the aluminum rod has been tested only in a wind-rod respective perpendicular direction. Results comparison for different angles should be evaluated in future projects in order to evaluate the increased effect on the turbulence of stranded conductors.

3.8 Conclusion and Future Works

The performed laboratory at KTH has been the first of a series of tests aiming to simulate OHLs conditions employing a closed wind tunnel. The laboratory results show that the effect of the change in the wind angle has a higher magnitude respect the one foreseen by the IEEE thermal model. This, preliminary, confirm the stated hypothesis. However, due to the high difference between test and model results it is not possible to understand in what extent the set up imprecision affected the obtained measurements. Different imprecisions derived from the simplicity of the used set-up. In order to obtain data valuable to find a precise answer to the initial objectives it is necessary to increase the precision of the laboratory equipment. Specifically difficulties have been experienced in the following procedures:

- Regulation of the current. Since no automatic control on the current has been employed, to maintain a constant value along all the measurements has been nearly impossible. The current decrease is related to the change of the conductor and copper cables resistance with the increase and decrease of the temperature. The same phenomena has been experienced in [21]. An example of the laboratory measurements is showed in Figure 14. In the example the current average value decreased of 2 °C in 5 minutes with an average error of +/- 0.5% . These imprecisions affect the thermal balance that take place between conductor and air, modifying the final steady state equilibrium. The actual magnitude of this effect can be calculated comparing the results with the one that can be obtained employing a current meter on the same set-up.
- Thermocouples precise installation. Differences of millimeters in the thermocouples positioning caused important differences in the results. It is suggested to carefully plan the sensors' position and to glow them directly on the conductor since wind flow, causing oscillations, affect the obtained results. An example of precise placement of the couple can be found in [35].The thermocouples were mounted in stainless steel sheaths, and attached to the conductor surface with aluminum tape.
- Precise regulation of wind speed. Wind speed has been regulated manually changing the fan rpm. This system proved to be quite accurate. An example is showed in the following graph.

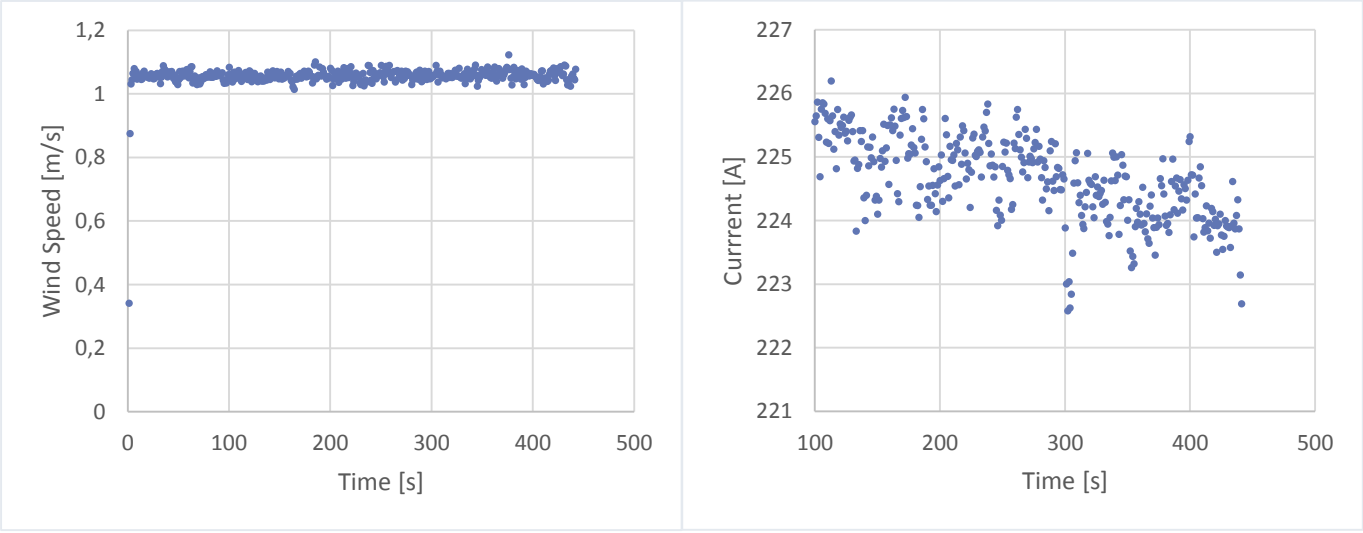

Figure 14: Examples for Wind and current stability during the cooling of AL59-20 at 1 m/s.

Another important factor to consider is the evaluation of the conductor tension. As reported in [30], [36], Tension has a relevant influence on the conductor radial temperature distribution. Future experiments should aim at the inclusion of load cells in order to simulate real line conditions.

4. DLR Equipment State of the Art

The possible economic advantages that grid owners can obtain through DLR exploitation triggered the development and commercialization of different monitor devices able to detect the necessary parameters for line rating calculations [37].

A vast and extensive set of components is available nowadays on the market. Differences between them lay on the estimated parameters. This chapter will give an overview of the different possibilities that TSOs and DSOs have to upgrade their OHL networks.

In order to evaluate the loadability of a line is necessary to know the state of the conductor and of the environment where it is located. Important weather and conductor parameters are reported in the following table.

Table 5: Weather and conductor parameters.

Weather Input	Conductor Input
Air Temperature	Conductor temperature
Wind speed	Current
Wind Direction	Voltage
Solar Irradiation	Sag \ Clearance to ground
Humidity	Tension

The correct combination and elaboration of these variables throughout the time allows to estimate the actual ampacity of an OHL in each single moment. Hereafter a review of the several solutions available on the market is presented. The list is divided by the kind of monitored data.

4.1.1 Weather Assessment Equipment

Dynamic line rating by weather monitoring represents the simplest solution. It is not invasive since nothing has to be applied directly on the line and needs a cheap set of measuring tools since the market of weather sensors is already a reality. The simplicity of the system is even-up from the imprecision that will characterize the obtained rating. Weather data will be measured in a slightly different place in respect to the actual line location and this will incur in discrepancy between the estimated and actual conductor situations. Moreover variations in the terrain and wrong forecasting of weather patterns decrease the reliability. In general, lines placed in microclimates cannot be rated properly only by weather measurements. A different system respect the typical weather stations, ThermalRate™ Monitor, is presented.

ThermalRate™ System

ThermalRate™ Monitor (**TRM**) is a weather-based sensor developed by PIKE, an U.S corporation. The device is based on an easy but effective concept. As it can be seen in Figure 15 the sensor is placed in proximity of the line (same height and direction) and it is composed of two replica sections. Both have the same conductor's outline, specifically they have identical dimensions, material and a similar surface. Both replica includes an embedded temperature sensor, and one of the replica sections contains an electric heater. In the lower part of the two replica is present a sensor called Thermalrate™ controller, It measures the temperature of the two sections and determine in this way the total effect of the environment in the line cooling and heating (effective wind speed and solar heating). This is possible because the difference of the measured temperature between the heated and not heated sections gives an understanding of the overall thermal rate exchange between sensor and environment. The relationship between conductor temperature and wind is identified by IEEE-738 standard. The effective wind speed also takes into account the various forms of precipitation. The TRM then calculates the actual rating of the line using the effective wind speed and the other parameters of the line conductor . [38]

Figure 15: Thermal Rate Monitor [38].

The complete ThermalRate™ system includes a radio modem communicating the rating information to the SCADA system center. It is necessary to only add a receiving radio unit in the substation center. No software changes are required in SCADA, since the TRM calculates the rating itself. ThermalRate™ system has low cost and simple installation and maintenance; it can be placed without causing an outage on the line (since it is not directly applied on the conductor). The only disadvantage is that it needs an energy supply unit, normally a PV panel. In addiction there is the need for a high number of sensors to obtain correct results since weather conditions may be very different along the line span. Typically, the recommended distance between two different sensors is 10 km [39], [40].

4.1.2 Conductor Assessment Equipment

Tension and Sag Monitoring

It is of paramount importance to control the sag of a line since, respect limits on clearance-to-ground status, means ensure a safe operation of the transmission and distribution lines.

Tension and sag values are directly related to each other. The sag of every line span is inversely proportional to the horizontal component of the tension. Specifically, sag, and therefore clearance status, can be obtained from line tension, span length and weight of the conductor [38].

One advantage of the tension and sag monitoring is that these parameters are associated with the average temperature of the conductor and not with a local measurement. This will give a broader understanding of the line situation without being affected by local microclimate that can be created by local forest shading or ground turbulence creation [38].

CAT-1

CAT-1 has been developed by Nexans. CAT-1 connects the conductor to the tension pole (Figure 16, right). In this way it measures the line tension and ambient weather parameters. Over 300 CAT-1 have already been deployed in North American and European transmission grids [41].

Figure 16: CAT-1 installation. PV panels are placed on the support tower to power the device [38].

The sensor is coupled with a software called Intelli-CAT; the overall system can calculate conductor temperature, sag, and trends in tension providing advance warning on clearance violations. The system also includes other two components CAT-PAC and CAT-Master.

CAT-PAC is the energy supply unit. The power is delivered by small PV as it can be seen in Figure 16 (left). CAT-Master is the elaboration unit placed in the base station. It receives data by 900MHz radio signals or by GPRS. It makes the outputs compatible with the EMS/SCADA system. [38]

The system normally also includes a Net Radiation Sensor (Figure 17) [37]. It is similar to TRM. It consists of an aluminum tube with the same emissivity and absorptivity values as the conductor. It is installed in the same tower where the load cell is installed. The tube is placed parallel to the conductor. A temperature sensor measures the temperature of the aluminum tube. This

temperature represents the temperature that the conductor has with no current intensity. Through this sensor it is possible to evaluate the weather conditions in an indirect way.

Figure 17: Net radiation sensor [38].

The total CAT-1 system analyze all the available information and calculates the available ampacity for the considered line. This solution is reliable and precise, Nevertheless some disadvantages are present:

- Necessity of calibration process to understand the Temperature-Tension curve.
- Installation requires outage and the dropping of insulators string.
- Data transmission intervals are long 10-15 minutes due to conductor thermal time constant.
- Necessity to apply different weather stations along the line.

ADR sense

ADR Sense is a DLR device produced by the Belgian company called Ampacimon. ADR calculates the sag (s) from the fundamental vibration frequency (f_1) of the conductor. The formulas used to obtain the sag value are shown below [42]:

$$f_k = \frac{k}{2L}\sqrt{\frac{T}{m}} \qquad (16)$$

$$s = \frac{mgL^2}{8T} \qquad (17)$$

$$s = \frac{g}{32 f_1^2} \qquad (18)$$

Vibrations are induced mainly by wind and thermal elongation and this means that from the induced frequency is possible to extrapolate the wind speed that exactly impacts the conductor and its temperature. This is done through a software developed by the same company. The device is self-powered by the conductor magnetic field and connected to the data center with GSM connection.

Figure 18: Ampacimon's device installation [38].

In Figure 18 it is possible to see how ADR Sense is applied to the conductor. This product has several advantages respect the competitors:

- No need for calibration or precise information about the conductor;
- Exact wind speed estimation on the conductor. It is essential to know exactly the wind magnitude on the line since as explained in the chapter also small variations can have a big important on the conductor cooling;
- High precision;
- Easy installation and maintenance.

Span Sentry

Span Sentry, previously called Sagometer [43], is a sag control device developed by Avistar. This system is based on image processing. As it can be noticed in a target is hanged on the conductor in the middle of the span and a camera situated on the tower locates the target and calculates the sag. Additionally, to calculate the rating of the line, the system is equipped with a current sensor, a weather station and a control box. The complete system is connected to the central station by GPS, GSM, radio communication or fiber optic. All the components can be fast installed without requiring the outage of the line (Avistar declares that the installation requires less than 3 hours [44]).

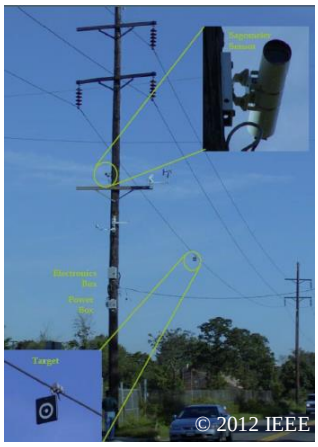

Figure 19: Span Sentry camera and target [38].

Promethean Device

Promethean DLR device [45] is a different non-contact sensor. In fact the system uses the AC magnetic field produced by the conductor to derive three phase currents, conductor clearance and maximum temperature. The temperature is calculated from the clearance to ground value. The system components are located under the three different phases of the OHL and each sensor (a pair of coils) detects the magnetic field of one of the phases. For protection from weather and vandalism, the sensors are buried as it is showed in Figure 20.

Figure 20: Promethean sensor position and burial [38].

The system is powered by two 85 W solar panels, with battery backup, and it establishes the communication with the operation center through a normal mobile phone connection.

The following product data sheet is available:

Table 6: Promethean device specifications.

Measurement	Accuracy	Notes
Conductor Height	+\- 0.12 m	at 18.5 m
Temperature	+\- 7 °C	
Current	+\- 22 A	at 830 A
Update rate	each 10 s	
date latency	60 s	

A calibration process is necessary to calibrate the sensor to line's height and current calculations.

Conductor Temperature Monitor

Conductor temperature is monitored by sensors installed directly on the conductor itself. The measured temperature is the result of the heat balance that take place on the conductor. Temperature monitoring allows to directly check limits on annealing and ground clearance. Ground clearance status is obtained from the sag magnitude. Sag can be obtained knowing temperature and span geometry. As it has been explained on the above chapter sag is function of the average temperature whereas the monitoring system gives a local temperature value. Thus, in order to safely monitor the line, it is recommended to place the device on the different hotspots of the OHL. [46]

In order to calculate the ampacity of the line the weather condition have to be known so normally a weather station is installed close to the line. [38]

Additional errors can be a consequence of the fact that normally, on the conductor, a radial temperature profile is present. This means that knowing the surface temperature value does not give a complete overview of the conductor state. [30]

Power Donuts

Power donut (PD) has been the first commercialized device for OHL temperature monitoring. It consists of a toroid applied directly around the conductor. The energy needed to power the sensor is harvested from the oscillating magnetic field created by the line's AC flowing current. PD has been developed and commercialized by Nitech in 1991. It is owned by USi-Power that refined the product and supplied the second and shortly the third versions, PD-2 and PD-3. The latest versions are able to calculate conductor temperature, current, voltage, I-V phase angle (and so MW and MVar) and line inclination. It stores data on board, and it transmits them on demand using a GSM/GPRS wireless data service. [47]

Figure 21: PD layout (left) and line installation (right) [38].

Knowing span geometry, donut's position and inclination it is possible to calculate the sag of the line and therefore the clearance to ground. The multiple outputs obtained by this device make of it an interesting option in respect of the competitors' DLR equipment. With a single donut on a line

it is possible to obtain conductor temperature, current and line sag. PD, coupled with weather measurements, and in communication with the SCADA system and substations' CPU, proved to be a reliable choice for DLR applications. The first DLR applications for OHL employed this setup.

The Data sheet of PD-3 is still not available on the company website. The following tables resume the second version main characteristics.

Table 7: Power-Donut specifications [48].

Physical	
Diameter	32 [cm]
Width	14 [cm]
Weight	9.5 [kg]
External Temperature	from -40 to +60 [°C]
Max Conductor Temperature	150 [°C] *
Max Voltage	500 [kV]
Nominal current	60 [A]

Battery	
Type	Li-ion
Discharge -time	10 Hr
Charge Time	6 Hr when current > 120 [A]

Precision	
Current	+/- 1% of the reading
Voltage	+/- 2% of the reading
Temperature Resolution	0.1 [°C]
Temperature Accuracy	+/- 1 [°C]
Inclination Resolution	0.01 [°]
Inclination Accuracy	+/- 0.05 [°]

Communication	GSM/GPRS
Software	Windows based

To conclude ,another important advantage of PD, is that it can be applied on the line without the need for a scheduled outage. This make the operation fast and economical. In the technical data-sheet is also reported that PD is "virtually maintenance free".

SMT and EMO

Other two similar products are under development and are now facing the commercialization step. One is called SMT [49] (Temperature Monitoring System) developed by Arteche and the other EMO [50] (Easy Monitoring Overhead Transmission) produced by MICCA. SMT has a compact design and measure temperature up to 120 °C while EMO obtain the conductor temperature through a more sophisticated manner. It has three sensors on the conductor plus a reference one. This allow a precision of 1,5 °C and a maximum temperature of 210°C. [50]

4.2 European DLR usage

Several DLR technologies have been tested on the field and are employed by several system operators around the world. Specifically, in Europe, 15 TSOs have been part of a survey conducted by ENTSOE [51]. European TSOs reported information about their use of DLR. Results of the survey are described in Table 8.

Table 8: ENTSOE report on European DLR usage [51] .

Status of DLR-projects	Used technologies	Output and usage of DLR
11 - TSOs have DLR in operation	**9** - TSOs use meteorological data from meteorological stations	**9 -** TSOs only for information
5 - TSOs have DLR in test phase	**6** - TSOs use temperature or current sensors	**13 -** TSOs for alarm to dispatcher
9 - TSOs are planning to use DLR	**3** - TSOs use a thermos-mechanical model	**0 -** TSO for trip (no automatic trip)
	2 - TSOs use a measurement of wire slack	**6 -** TSO with other actions (e.g. limits for EMS)
	1 - TSO uses fixed limits acc. to the seasons (winter / summer)	
	3 - TSOs use Synchro-phasor data from PMUs	
	1 - TSO uses a vibration measurement	

It can be concluded that DLR devices are already operating in several European grids. One important detail to notice is that none of the TSOs uses DLR for automatic trips. System operators use DLR only for information and alarms. This shows that the different devices still have to prove to be completely reliable to work without a careful monitoring by the operation center. [49]

4.3 Alternative to DLR

Avoid power capacity limitations is essential for DSOs and TSOs since bottleneck effects can incur in expensive fees [24]. Therefore, also a small increase in the capacity of overhead lines, may have a significant positive economic impact. DLR is not the only solution to upgrade transmission or distribution lines. In general two different upgrading possibilities can be classified [52]:

- Ampacity increase;
- Voltage increase.

Increase the voltage level requires high investment costs [52]. The electrical isolation has to be increased and the towers and foundations need to be reinforced. Besides the changes on the line components, the substations equipment has to be adapted to the higher voltage level too. For this reason this solutions is employed only when the rating increase is high enough to justify important investment costs.

Applications of this method can be found in [53]–[55]. These examples correspond to different countries such as USA [54], [55]and Germany [53]. The following table shows the different results.

Table 9: Voltage upgrade results comparison.

Case	Increase in rating (%)	Saving from upgrade (%)
V2 [55]	-	40
V3 [55]	-	45
V4 [55]	-	45
V5 [55]	-	50
V6 [53]	217	32
V7 [53]	200	42

Ampacity can be increased through different approaches.

The first option is to increase the conductor section. A bigger section means a lower resistivity, thus, a higher ampacity. The conductor replacement results in necessary changes in insulators, towers and foundations. Insulators have to be adapted to the new conductor configuration since the increase in section results in a weight growth. For this reason, the mechanical requirement of the towers is increased and normally a reinforcement is needed.

Examples are analyzed in [53], [56].[53] Report a German case while [56] include a Spanish application. Results are presented in Table 10.

Table 10: Ampacity upgrading results comparison.

Case	Increase in rating (%)	Saving from upgrade (%)
S1 [53]	31	53
S2 [56]	100	-

The second and more expensive possibility consists on the construction of a new line in parallel with the old one. This option is normally avoided because of the related economical environmental and social issues [24].

Another way to increase the ampacity is to increase the allowable conductor temperature. Normally the temperature constraints are driven by clearance to ground limitations [52]. If this is the case mainly two different solution can be adopted:

- Increase the height of the line.

This can be achieved by the increase of the towers height, increasing the line tension or replacing the insulator strings. Examples can be found in South Africa where 400 kV line with 50 ºC limit have been upgraded to 85 ºC with a rating increase of 60 % [57] With an investment equal to 5% of the original one. Another UK application is analyzed in [58]. ACSR OH lines maximum temperature has been increased form 50 ºC to 75 ºC achieving a rating increase of nearly 25 %.

- Replacement with low-sag high temperature conductors [59].

This approach allows considerable loadibility improvements without the need for modifying the line's supports. These conductors experience a small elongation at high temperatures. Then, for the same sag limitations, a higher conductor temperature is allowed. The higher is the temperature limit, the higher will be the tolerable current. There are several types of conductors available; examples are: TACSR, GTASCR, ZTACIR, ACSS. These conductors can work between 150 and 250 °C without mechanical or chemical modification of their molecular structure.

TACSR conductor (Thermal Resistance Aluminum Alloy Conductor Steel Reinforced) has a steel core with TAL (Aluminum-Zirconium alloy that have stable mechanical properties up to 150°C) wires around it. [59]

GTACSR (Gap-type Thermal Aluminum Conductor Steel Reinforced) is a type of conductor that has a small gap between steel core and aluminum outer layers. The gap is filled with heat resistant grease (filler).The grease decreases the friction between core and outer layers and prevent water penetration. In this way the tension is applied only on the Extra high-tensile galvanized steel core and higher working temperatures are allowed. [59]

ZTACIR (Super Thermal Aluminum Conductor Invar Reinforced) conductor consists of steel-invar galvanized alloy core and ZTAL strands in the outer layers. It is annealing resistant up to 210 °C. [59]

Also ACSS (Aluminum Conductor Steel Supported) presents a steel core surrounded by annealed aluminum strands in. [59]

Applications are described in [60]–[62]. In the UK case, the replacement of the conductors on a 400 kV line by GZTACSR resulted in an loadibility increase of 130 % [60]. In Spain, the substitution by GTACSR increased the rate of 70 % for a 132 kV line [61]. The replacement by ACSS/TW of a 138 kV line in the USA resulted in an increase of 70 % in the ampacity [62].

4.4 Ethical aspects

DLR allows to contain respect the traditional upgrading solutions the environmental footprint due to the introduction of new power units into the grid. Different ethical advantages are present as listed below:

- Avoid the utilization of an important amount of metals. The new line construction or conductor substitution are raw material intensive processes. As an example, the conductor of the selected study case, has a specific weight of 817 kg/km [Appendix A]. Wider sections incur in heavier lines. OHL conductors are mainly composed of aluminum strands. Both the extraction (up to 50 GJ/ton) and the recycling (From 3.5 to 16.5 GJ/ton) of this metal are high-energy intensive processes. Avoiding the need for a large amount of aluminum strands decrease both the resource and energy footprints[63].
- Avoid the forest destruction necessary to introduce a new power line in the environment.
- Allow a fast introduction of renewable energy plants. The construction of a new line can take up to 10 years only to obtain the permission [52].

5. Study Case

Swedish installed wind power is expected to reach 6466 MW by the end of 2016 [64]. This power will be supplied by 3382 turbines spread on the Swedish territory[64]. As it can be noticed in Figure 22 the turbines' distribution is uneven. Favorable wind conditions are found mostly in the southern part of the country [65].

Värmland region is located in the South-West area. Ellevio AB owns different lines located in this territory and will need to face the installation of new wind power capacity in the coming future. Two OHLs will be analyzed to estimate the impact of DLR installation as a mean to accommodate higher current levels in pre-existing networks. These two OHLs are in this work named line A and line B.

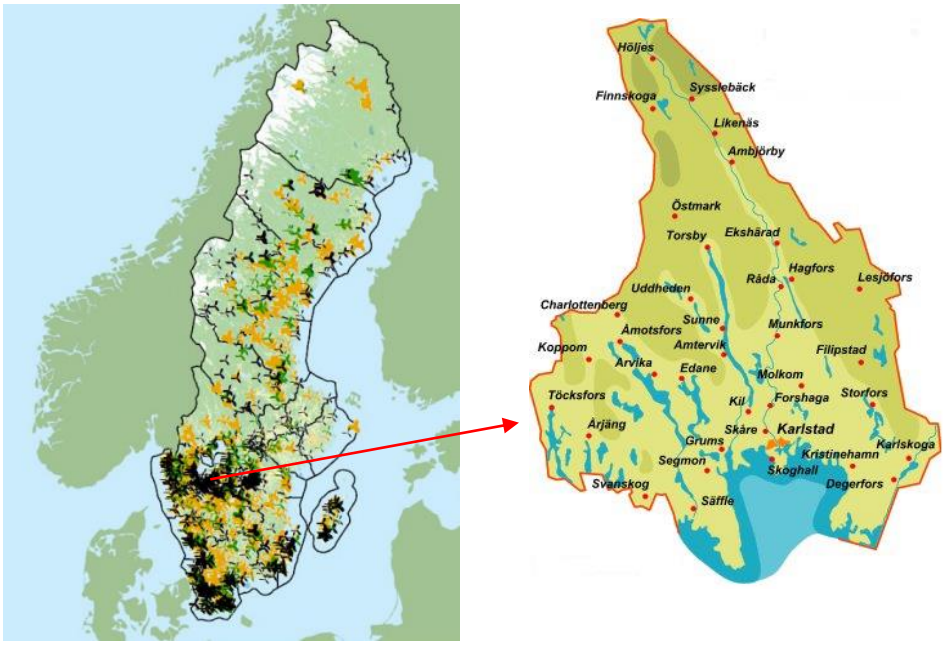

Figure 22: Swedish wind turbines installation overview. Black-Installed, Yellow- Approved, Green- New. On the left Värmland region is depicted [64].

5.1 Regional Weather

The OHLs are situated approximately 100 km far from the sea and between 100-200 meters above the sea level. Thus, the climate in the region can be considered continental, with cold winters and warm summers. Meteorological site data have been provided by Ellevio AB. Weather measurements from the area show that the main wind direction is from South-West.

The wind speed distribution shows that the average wind speed is 6 m/s. The time with wind speed higher than 10 m/s has been 8% of the total measurements time.

This condition depicts an ideal location for wind energy exploitation. For this reason different turbines are already installed in the area and farm owners are interested in increasing the overall installed power. In Årjäng two wind farms are already present, with a total installed power of 68 MW [66].

The investigated OHLs cross different terrain conditions, from open hills to forests. Line B passes also over a public road. Different places incur in different microclimates and constraints. This lead to the unavoidable research of the most sensible spans of the OHLs.

The correct identification and protection of the critical span would guarantee the safe operation of the entire line.

As cited and demonstrated by the experiment, convective cooling has a major contribution in the total heat transfer of the OHL conductor. This suggests that location with low wind exposition have the prerequisite for being hotspots.

Average wind measurements are available from both the vicinity of the farm (Årjäng at 100 m height) and of the OHLs (Arvika at 10 m height). The two sites are approximately 40 km far from each other. In order to understand the relation between wind energy supply and OHL cooling magnitude, data from the two locations are compared to analyze the correlation between the wind condition in the different locations.

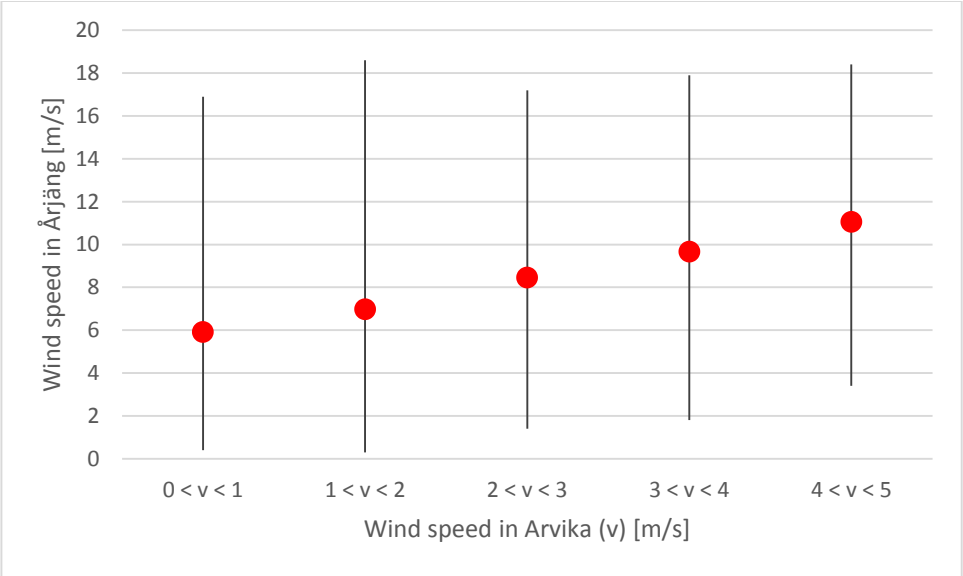

Figure 23: Correlation between the wind speeds measurements in Årjäng (hub turbine's height) and Arvika (10 m) during 2015. The red points represent the average speed and the vertical lines the whole correlation range.

The above graph depicts how, in average, a satisfactory correlation between the wind speed in the two different locations is present (usually a higher wind speed at the turbine location coincide with an increased wind speed in the OHL area). It is important to notice that several possible risky conditions have been registered along the year. It is possible to notice how, a wind speed of 16.9 m/s, enough to fully power a standard wind turbine, co-existed with moments of still wind conditions at the OHL location. In these instances, the increase in the line current, is not correlated with an increase conductor cooling. Thus, during these periods, overloads of lines are possible and this remind how important is the monitoring of the network conditions.

Considering that these critical events have been recorded only during few occasions it can be concluded that generally a higher wind energy supply coincide with an increased cooling capacity.

Also, the thermal effect due to an increased wind power supply is not directly proportional to the effect of the increased wind convective cooling. It is important to notice that, as it has been

demonstrated by the experiment, the difference between a wind speed of 0 and 1 m/s would incur in an important increase of the cooling capacity. In addition, the difference between a perpendicular or parallel direction respect wind and conductor has a substantial impact on the overall cooling process. Employing the IEEE thermal model standard the following results are found.

An "Ibis" ACSR conductor in an ambient temperature of 22 °C is considered. The increase of the wind speed from 0 to 1 m/s make the cooling capacity grows from 5.8 W/m to 44.489 W/m (almost 7 times higher) increasing the current rating of 265 A.

For a wind speed of 1 m/s, the calculated convective cooling capacity of a perpendicular and parallel wind directions is of 44.49 W/m and 17.26 W/m respectively (2.5 times lower). This reduce the current rating of 170 A.

5.2 HOT-SPOT Identification

Analyzing the lines' profile in Figure 24 it is possible to notice how a small part of line B is in South-West direction. This means that the wind will flow parallel to this span for the majority of the time.

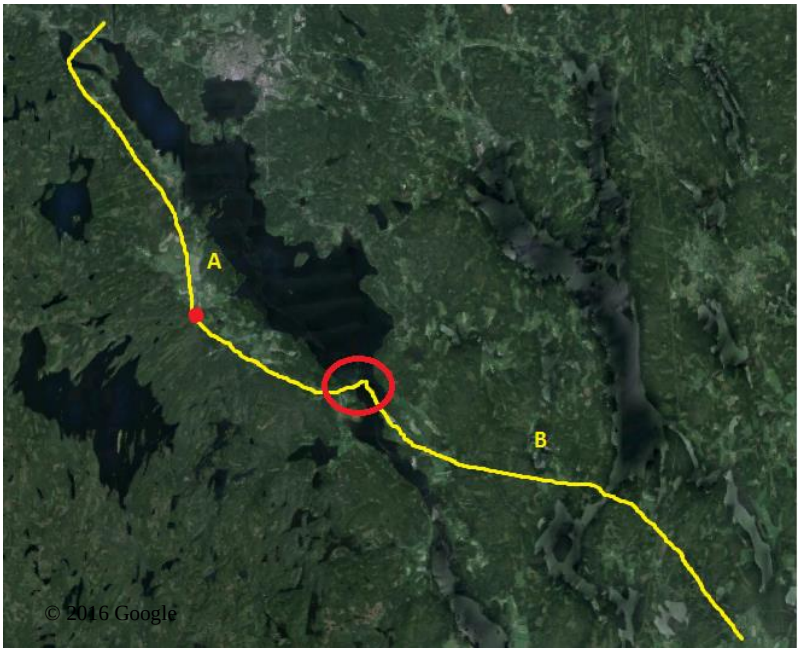

Figure 24: Lines A and B profiles. North is located on the higher part of the picture. [67]

In addition, forests are present in the area. The presence of high trees creates wind shadowing effects on the line reducing the effective wind speed hitting the conductor. Ellevio AB identified this location (marked with a red circle in Figure 24) as one of the hottest sections of the line, i.e. the critical span that will be further analyzed.

Historical weather data from the precise location have been analyzed to better understand the average conditions experienced by the sensible span. Weather data have been taken from the NASA Surface meteorology and Solar Energy Archive [68].

The wind measurements are available at 50 meters height. In order to obtain valuable data for the conductors actual height, the NASA data have been scaled down. The data available in Table 11 are related to a height of 10 meters in an area characterized by a 2.5 surface roughness class. The roughness length (Z_o) for this class is considered 0.2 m [69]. The wind share for a 2.5 surface roughness class is shown in Figure 25.

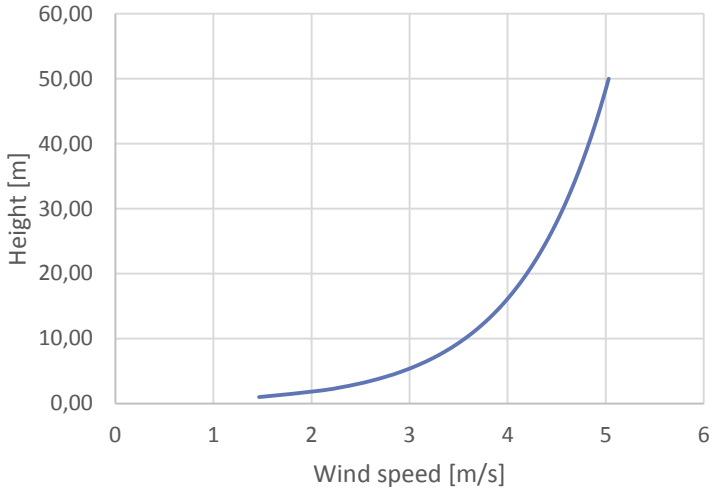

Figure 25: Wind share for 2.5 surface roughness class.

The scaled wind speeds results are obtained through the following formula:

$$V(h') = V(h) * \frac{\ln\left(\frac{h}{Z_0}\right)}{\ln\left(\frac{h'}{Z_0}\right)} \qquad (19)$$

Table 11 and Table 12 reports respectively the average data for wind speed and direction at 10 meters height (Latitude 59.5; Longitude 12.5).

Table 11: Monthly average wind speed for 3-hour intervals of GMT during a given month, averaged for that month over the 10-year period (July 1983 - June 1993). Wind speed values are for 50 meters above the surface of the earth.

Hour	Jan	Feb	Mar	Apr	May	Jun	Jul	Aug	Sep	Oct	Nov	Dec	Annual Average
01:30	3.97	3.72	3.59	3.37	3.34	3.30	3.25	3.24	3.63	3.73	3.81	3.84	3.56
04:30	3.99	3.69	3.52	3.20	2.81	2.42	2.49	2.78	3.42	3.67	3.78	3.75	3.29
07:30	3.99	3.60	3.07	2.30	1.96	1.87	1.90	1.77	2.47	3.37	3.68	3.70	2.80
10:30	3.71	2.83	2.74	2.76	2.76	2.59	2.68	2.58	2.69	2.79	3.17	3.48	2.90
13:30	3.55	2.77	3.20	3.09	2.99	2.76	2.95	2.90	3.24	3.09	3.00	3.37	3.07
16:30	3.92	3.39	3.37	3.09	2.98	2.74	2.97	2.97	3.36	3.48	3.58	3.66	3.29
19:30	3.97	3.74	3.71	3.28	3.05	2.75	2.92	3.15	3.73	3.89	3.78	3.74	3.47
22:30	3.95	3.75	3.73	3.47	3.43	3.29	3.33	3.40	3.80	3.88	3.78	3.80	3.63

Table 12: Monthly average wind speed for 3-hour intervals of GMT during a given month, averaged for that month over the 10-year period (July 1983 - June 1993). Wind speed values are for 30 meters above the surface of the earth and third Roughness class.

Hour	Jan	Feb	Mar	Apr	May	Jun	Jul	Aug	Sep	Oct	Nov	Dec
01:30	277	273	220	27	332	327	291	268	277	233	282	278
04:30	279	282	234	15	350	2	313	299	293	240	292	284
07:30	277	281	228	19	2	40	318	290	300	241	300	284
10:30	271	266	206	68	289	139	262	221	272	233	297	278
13:30	271	251	213	133	244	219	255	227	253	229	287	277
16:30	274	255	211	48	269	250	264	234	254	220	292	280
19:30	271	258	208	95	268	222	264	231	252	217	287	273
22:30	272	259	213	95	282	193	269	238	261	223	277	271

The average wind direction is 278°. This value is close to the span orientation (11° difference).

NASA archive data on the span location confirm that there is a risk for the selected sensible spans because of the line average wind parallel directions. The significant average wind speed along the year also justifies the investigation of DLR as a mean to increase the loadability of the selected OHLs.

5.3 DLR Analysis

To understand how the span behaves in different climate conditions line and weather data have been precisely monitored and analyzed along the entire 2015 year.

The collected data include:

- Line current. The data is obtained from active power measurements on lines A and B.
- Three hours interval weather data. Temperature, wind speed and direction have been retrieved from Arvika SMHI weather station [70]. The weather station is 18 km far from the hotspot.
- Conductor characteristics. The employed conductor is called Ibis. It is an ACSR conductor with an overall area of 234 mm^2. More information on the conductor can be found in Appendix A.

Weather data are depicted in the following graphs.

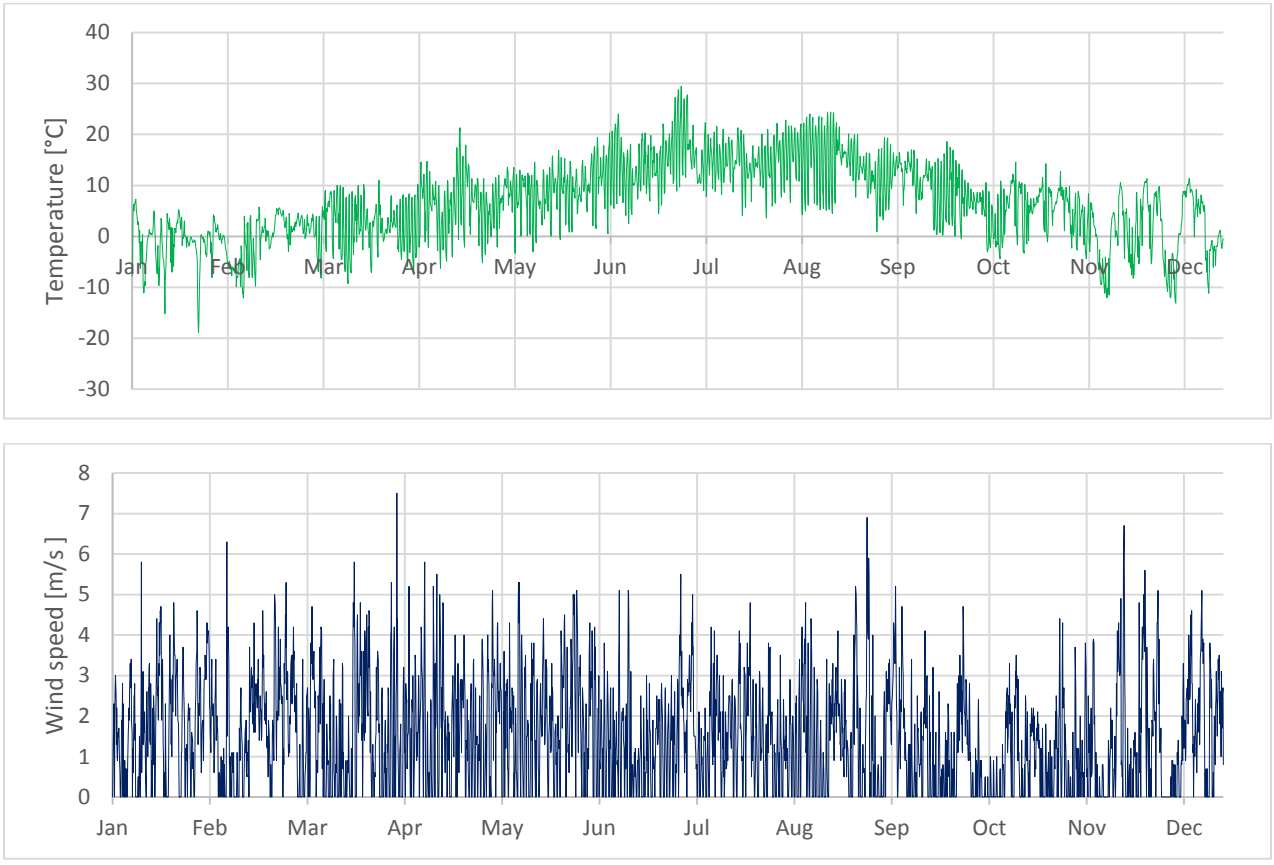

Figure 26: Registered wind speed and ambient temperature in 2015 from SMHI Arvika weather station.

The temperature ranged between 30 and -20 °C with an average of 6.63 °C. The registered medium wind speed is 1.5m/s. It reached peaks of 7.5 m/s. In Figure 27 it is possible to notice that there is no evident correlation between air temperature and wind speed during the selected period.

It is important to notice that clouds effect is not taken in account. Due to the high variability that the cloudiness level has, direct radiation is calculated all along the year without considering the clouds shadowing effect. This choice ensure that the obtained results are conservative.

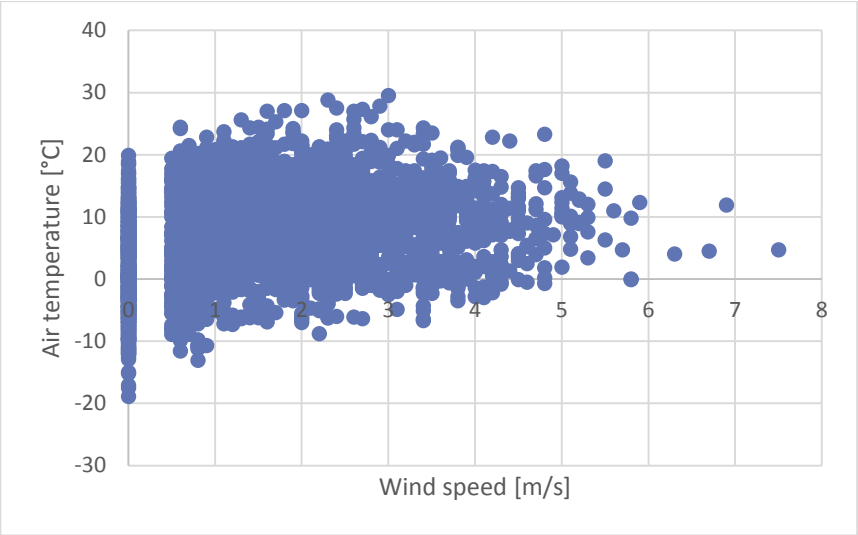

Figure 27: Correlation between ambient temperature and wind speed at Arvika weather station.

An Excel and Matlab models have been developed in order to estimate the line temperature during the selected period. Differently from the model developed for the laboratory data analysis, the latter calculates the current rating in steady state conditions.

The thermal heat rate exchange has been calculated following the IEEE 738 standard. The allowed maximum current is calculated through the following formula:

$$I_{MAX} = \sqrt{\frac{Pc+Pr-Ps}{R}} \qquad (20)$$

Where P_c and P_r are convective and radiative cooling, P_s is the solar heating and R the resistance of the conductor. To calculate the rating it is necessary to decide the maximum temperature that the conductor can withstand without incurring in annealing or clearance to ground issues.

For the selected line 50 °C is taken as the maximum allowed temperature. The selected line is rated with the SLR method. Two different limits are present, one summer and one winter rating. The maximum ampacities obtained for the two different periods are reported in the following table.

Table 13: Summer and winter static line ratings.

	Ambient temperature [°C]	**Wind speed [m/s]**	**Ampacity [A]**	**Period of validity**
Summer	30	0.6	**344**	1st of May to 30th of September
Winter	10	0.6	**531**	Rest of the year

To calculate the DLR it is necessary to estimate the actual conductor experienced weather conditions. The wind speed is scaled using formula 19 from a height of 10 m (Anemometer height at SMHI weather station) to a height of 6.4 meters. This value is the minimum allowed for the selected line. This ensure that rating calculations are conservative along the whole span's length.

The solar heating has been estimated using the direct radiation. To calculate the direct radiation component it is necessary to know the sun position along the selected period. This has been determined with the developed Matlab code. Figure 28 shows the differences between DLR, SLR and actual current flowing in the selected line.

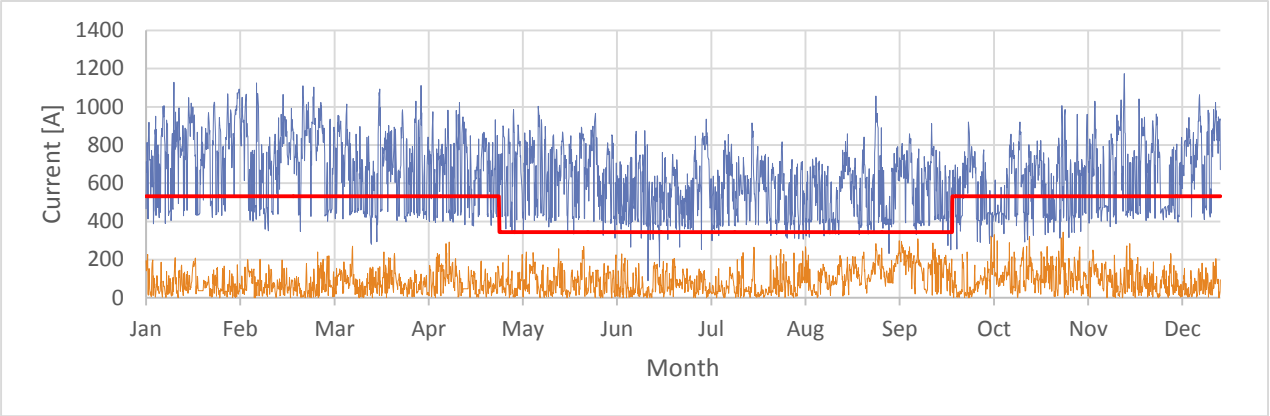

Figure 28: SLR (Red), DLR (Blue) and actual flowing current (orange) on the selected hotspot.

It can be noticed that that the model prediction crosses several times the SLR limits. This is an important result since SLR ampacities would cause conductor overheating in many different occasions.

However, the registered current along the year, has been way lower respect the static rating constraints. The current never went over the limits imposed by both SLR and DLR. The average DLR current value has been 550 A higher in respect to the average actual flowing current, and 183 A higher respect the SLR. This means that there is extensive room for the inclusion of new energy fluxes in the grid.

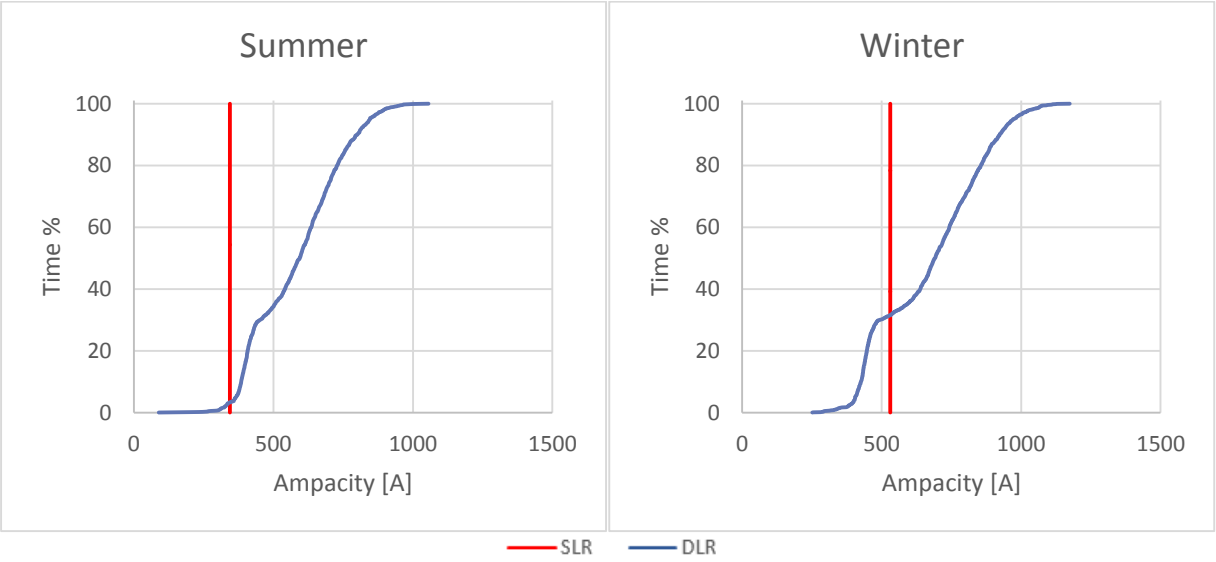

Figure 29: Difference between static and dynamic line rating in the different seasons.

The ampacity cumulative curve for line B is reported in Figure 29. DLR is compared with the static ampacities for the two different seasons. It is observed that the ampacity is underestimated for most of the time. Table 14 reports the resulting values that can be resumed from Figure 29.

Table 14: Uprating margin results for 2015.

	Time DLR > SLR	Medium ampacity improvement
Summer	96.5%	69.6%
Winter	68.0%	26.7%

During the coldest months, DLR has been lower in respect to the SLR for 32% of the time. This value is of concern since, if the load would reach the static maximum level, overheating issues would appear for a third of the total season length. The winter wind speed cumulative curve is reported in Figure 30. It can be observed that also the probability that the wind speed is lower than 0.6 m/s (Value estimated with SLR approach) is 30%. This suggests that the SLR wind speed choice is not conservative and remind the importance of the convective cooling component in the overall conductor thermal behavior.

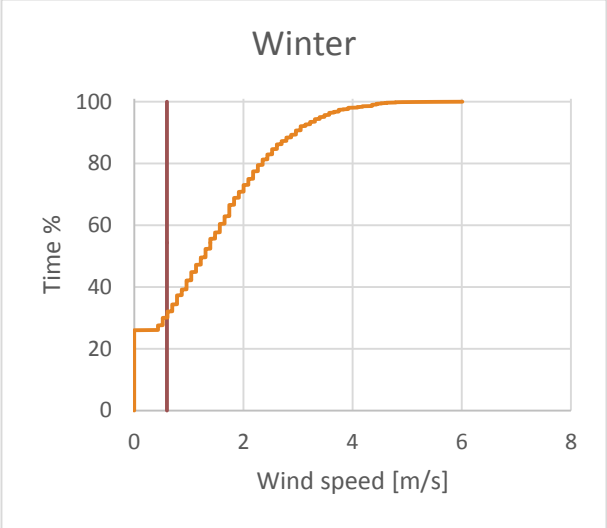

Figure 30: Winter wind speed probability distribution.

The next paragraph reports an example of the consequences that SLR ampacity overestimation can have.

Consequences on sag

In order to evaluate the SLR ampacity overestimation drawbacks, the developed transient thermal model is employed to simulate the conductor temperature response to an excessive current. The maximum difference between SLR and DLR along 2015 has been of 275 A. This happened in the morning of the 2nd of October 2015. Table 15 depicts the climate conditions present at that time. SLR overestimation is due to the presence of a lower wind speed and a higher air temperature respect the considered winter worst scenario.

It is assumed that the initial conductor temperature is 50°C. The transient is evaluated for 10 minutes. The results are depicted in Figure 31.

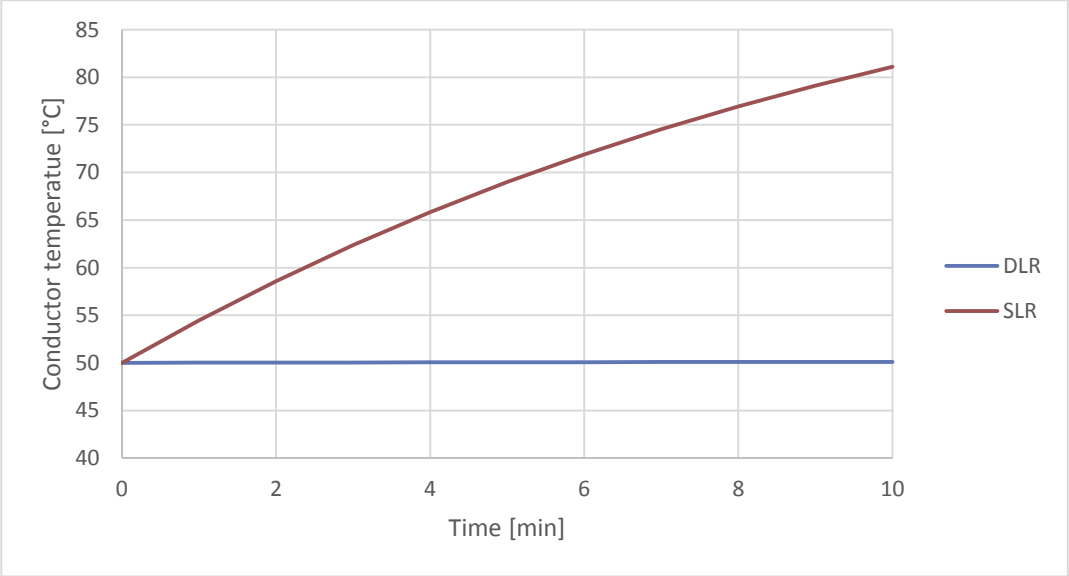

Figure 31: 10 minutes conductor thermal transient difference between SLR (531 A) and DLR (256 A) on the morning of the 2nd of October 2015.

If equation 3 is assumed valid for the hotspot span, the line would sag 1.15 m more than expected at the end of the 10 minutes. This value can become dangerous in case of the presence of public roads or other obstacles under the OHL.

Table 15: Climate parameters and calculate additional sag in the morning of the 2nd of October 2015.

Air Temperature [°C]	Wind speed [m/s]	Qs [W/m]	SLR [A]	DLR [A]	Sag difference [m]
11.1	0	12.98	531	256	**1.15**

In the reality no issues have been registered on the line since the current level has been low at the same time (3.26 A).

Since the calculations have been performed for the maximum registered overcurrent, the sag excess would have been less than 1.15 m along the rest of the year (considering a maximum thermal transient duration of 10 minutes).

K_{angle} effect

The master thesis project aimed at the verification of the coefficient K_{angle}. This parameter is employed in the forced convective cooling calculation of the IEEE standard. The laboratory imprecisions did not allow to have a precise understanding of the parameter accuracy. The following sensitivity study has been conducted in order to estimate the influence magnitude of K_{angle} on the conductor cooling. Results shows that the coefficient substantially influence the conductor's rating.

The following graph depicts the effect on the calculated DLR with a +/- 10% change of K_{angle} value.

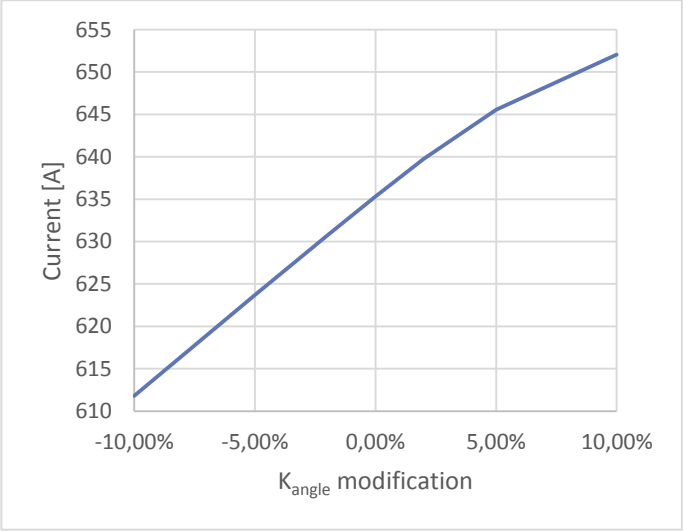

Figure 32: average ampacity rating modification due to a decrease or increase of Kangle.

A 20 % increase of K_{angle} make the average ampacity increase of 40 A circa (that for the investigated OHL corresponds to an increase of 9MW in the allowed power transmission). It is concluded that the effect of K_{angle} can have an important role on OHLs rating and further investigations should be conducted in order to better estimate the conductor conditions when the wind does not flow in a perpendicular direction.

5.4 New Wind Farm Installations

As it can been noticed in Figure 28, the current flowing on line B does not represent a risk for the conductor itself since both DLR and SLR are respected.

The situation could change if new wind power will be installed in the area. In order to evaluate this hypothesis, the installation of nine new wind turbines will be evaluated. The selected wind turbine type is Vestas 112. This wind turbine has a nominal power output of 3075 kW.

Data on wind turbines production have been obtained from Ellevio AB and Rabbalshedekraft.

It is assumed that in average 60% of the produced wind power will flow in line B (Ellevio AB measurements shows that in average 40% will flow in another line). With this assumption it is calculated that, in average, line B current increased of 26.5 A in respect of the load without the new wind farm. The yearly overcurrent is depicted in Figure 33.

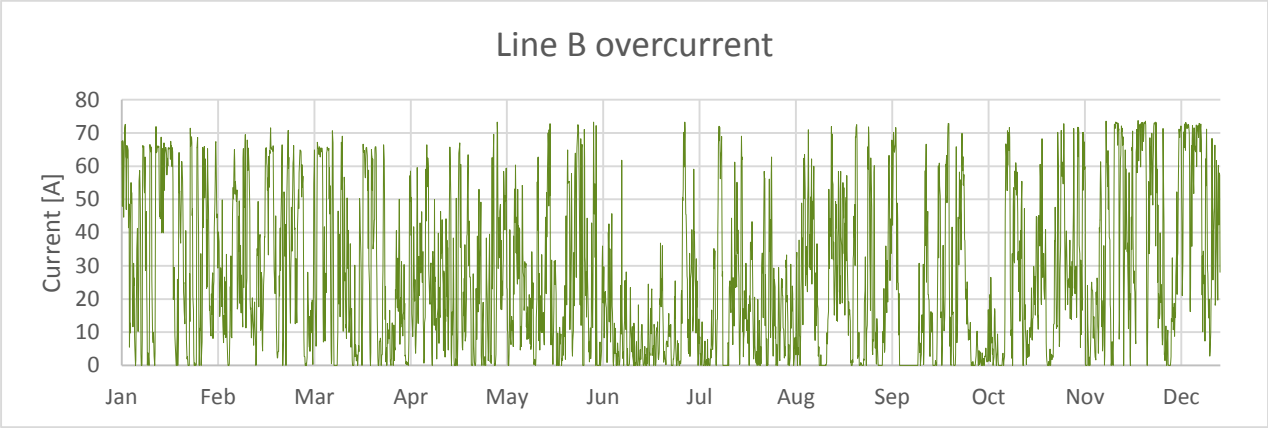

Figure 33: Line B overcurrent due to the new turbines installation in 2015.

Despite the new installed power, also in this case, the actual current is always lower than the DLR limits. This means that the installation of the wind farm would have not incurred in any overheating issues along 2015. This also means that no energy curtailment would have been necessary, allowing the complete exploitation of the renewable resource.

The same would have not been true if the SLR approach would have been adopted. The current went over the limit for a total of 12h hours causing the necessary curtailment of 37.41 MWh of wind energy.

The difference between measured current, DLR and SLR limits went below 50 A in 0 and 21 cases respectively.

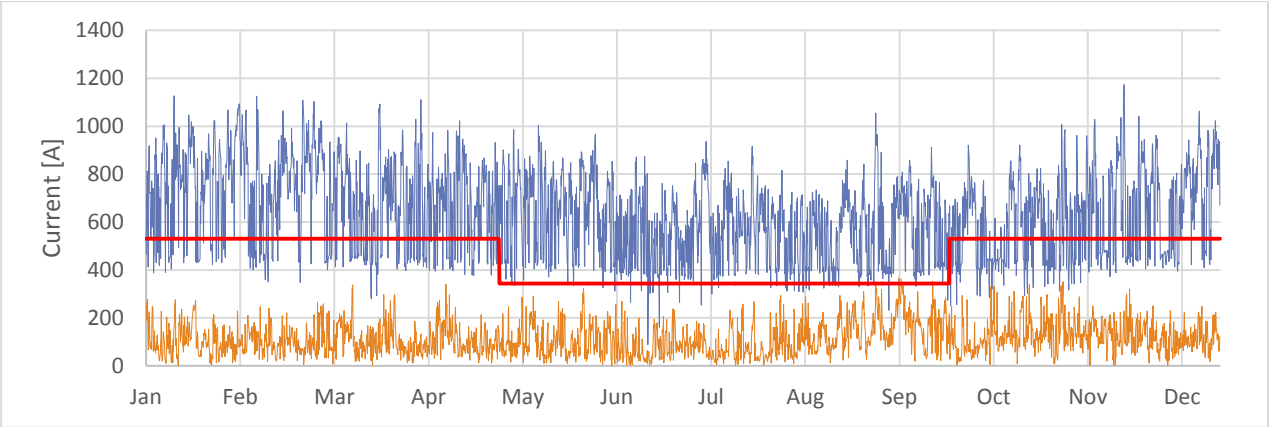

Figure 34: Updated current supply with the inclusion of nine new wind turbines.

In order to better understand the difference between dynamic and static line ratings, in cases of higher loads, a sensitivity study is performed. If more wind turbines would be installed in the same location the need for energy curtailment is expected to arise. The sensitivity study range between the installation of 9 and 54 new wind turbines. Figure 35 shows the difference between the necessary curtailment employing the two different methods.

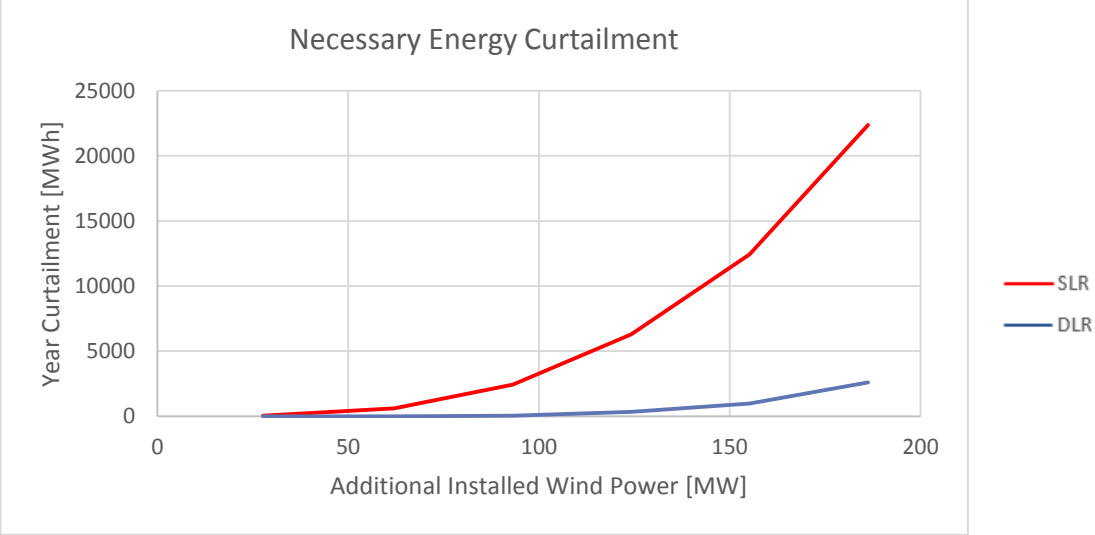

Figure 35: Increase in the necessary energy curtailment due to the installation of new wind turbines (SLR red, DLR blue). The analysis ranges between 9 and 54 new turbines.

It is possible to notice in Figure 35 that the difference between the two approaches is clear. Energy would be curtailed, employing DLR, from the installation of 27 new wind turbines (41.07 MWh). In the extreme situation of 54 new installed wind turbines the SLR energy curtailment would be 8.65 times higher in respect of the needed 2.56 GWh with DLR. Figure 36 depicts the case of the installation of 54 new Vestas 112 wind turbines.

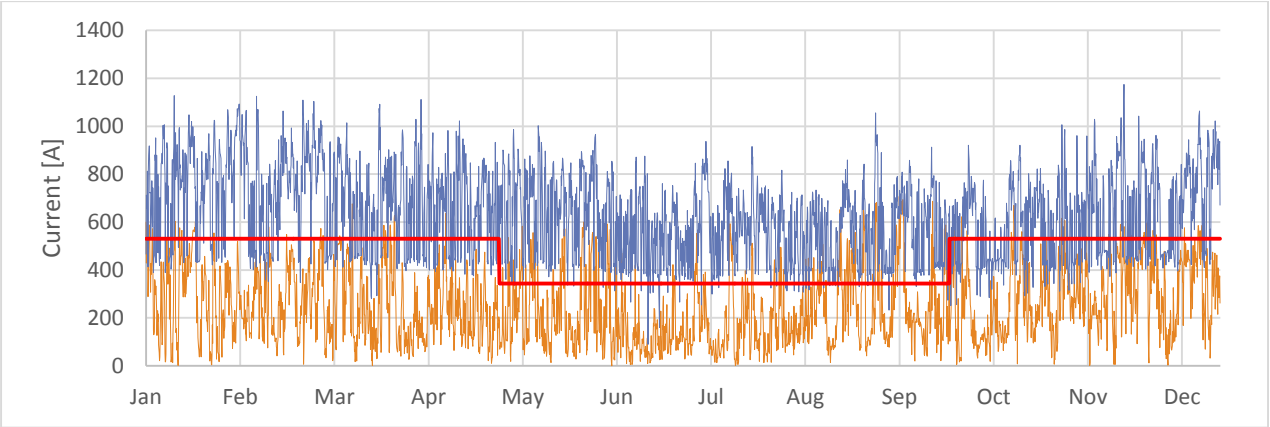

Figure 36: Updated current supply with the inclusion of 54 new wind turbines.

5.5 Technical Analysis Discussion

Calculations performed with the developed model proved that the installation of new wind turbines in the area would not incur in over-rating issues for the selected OHL. DLR would allow a substantial higher wind power penetration in the area in respect of SLR without the need for power curtailments.

The usage of SLR in addition, being based on a wind speed of 0.6 m/s, can represent a treat for the grid as it has been demonstrated in Figure 29. The treat is due to the possible increased sag magnitude that can be caused by unexpected conductor's high temperatures. The imprecision of the static approach can be the cause of clearance to ground issues since, as it has been demonstrated in Table 15, the line can sag up to 1.15 meters more than expected. An assumption of a constant wind speed of 0.6 m/s demonstrated to be not a conservative decision, even if the current never went beyond the limits during the analyzed year.

In order to increase the reliability of the proposed model it is necessary to employ more precise (from a location and time-span point of view) weather data for the OHL location. If the time span would decrease to the order of minutes it would be possible to use the transient instead of the steady-state thermal model and obtain detailed information on the conductor behavior along the time.

Since the selected span is connected to a tension pole, from a technical point of view, it is suggested to use a tension monitoring system since it would allow to have both a direct understanding of the sensible span sag conditions and the control of the entire line length. This is important since the area is characterized by the presence of different forests that have a high wind shadowing effect potential.

The next chapter will analyze in economical terms what will be the benefit of different rating improvements for the selected study-case.

5.6 Economic Analysis

The technical analysis shows how the increased power flow due to new wind turbines installation would have incurred in OHLs overloading only during few hours of the selected period. Even if this statement has been true for the whole 2015 year, it is not possible to conclude that the line will not suffer of higher currents loading along the future operation of the system. In this scenario DLR seems to have all the prerequisites to be the best choice in order to accommodate new green energy in the system at the lower grid-owner expenses.

DLR in fact, allows DSOs to postpone or avoid the construction of new OHLs. Due to the multiple number of stakeholders present in the energy market it is difficult to estimate precisely the share of the benefits each actor will receive. Generally it is possible to affirm that DLR has the potential to:

- Supply cheaper electricity to consumers (a DLR advantage for society);
- Decrease the connection fees of wind power owners (in terms of lower connection fee);
- Improve the economic use of existing transmission lines ensuring a cost effective utilization of pre-existing assets (useful for the DSO);
- Avoid unnecessary load shedding under contingency conditions [18].

An economical investigation is below presented in order to estimate the benefit of DLR in respect of the other possible upgrade solutions. DLR will be compared to the substitution of OHL conductors and the construction of a new line in parallel. The economic investigation between the different cases will be analyzed using two different economic indexes: Net Present Value and Discounted Pay-back Period. The indexes will be shortly described below.

Net Present Value [71]

The NPV is the present value of an investment's expected cash inflows minus the costs of acquiring the investment. It takes in account the time value of money, in other words, it considers the fact that a coin today as a different value of the same coin next year. NPV is a useful tool to determine whether a project or investment will result in a net profit or a loss. A positive NPV results in profit, while a negative NPV results in a loss. NPV is calculated with the following formula:

$$NPV = CF \sum_{j=0}^{n} \frac{(1+f)^j}{(1+R)^j} - I_0 \qquad (21)$$

With:

$$(1+R)^j = (1+r)^j (1+f)^j \qquad (22)$$

Where:

- **f** inflation rate
- **R** Real discount rate
- **r** Nominal Discount rate
- **CF** Cash flow
- **n** Life time of the project
- **I_0** initial investments.

Discounted Pay-back Period [71]

The discounted payback period (DPP) is the amount of time that it takes to cover the cost of a project, by adding positive discounted cash flow coming from the profits of the project. It also takes in account the time value of money.

5.6.1 Input and results analysis

Results are sensible to the choice of the several inputs value. In particular, as said before, it is problematic to estimate correctly what will be DSO's benefit share subsequent to a line upgrading.

The comparison between the different solutions is based on the relation between the needed investments and the increased transmittable power upgrade.

Table 16 reports the data used for the loan and actualization calculations.

Table 16: Loan and actualization calculations input.

LOAN		Actualization		
Loan Length	**Nominal interest rate (R)**	**Cash Flow time**	**Nominal Discount Rate (R)**	**Inflation Rate**
20	0.062	20	0.062	0.02

20 year is expected as the DLR devices life time.

Interest and discount rates are assumed to be equal to the estimated weighted average cost of capital (WACC) that is 6.2%.

It is expected that the CPIF inflation (The CPIF is the Consumer Price Index with a fixed interest rate) will reach a steady value of 2% in 2017 [72]. Thus 2% is taken as the reference value for the calculations.

The resulting real Interest rates (**r**), calculated using formula 22, is equal to 4.1%.

Costs

Table 17: Upgrading methods specific costs

DLR				Traditional	
Weather Station [kSEK/station]	**Power Donut [kSEK/hotspot]**	**CAT-1 [kSEK/km]**	**ADR Sense [kSEK/hotspot]**	**Conductor Substitution [kSEK/km]**	**New line [kSEK/km]**
100	510	23	350	1235.109	1483.521

Line B is approximately 40 km long. This value is employed to obtain the total cost for CAT-1, substitution and new line uprate methods.

The first hypothesis is that PD and ADR Sense will be installed only in the selected hotspot. PD, ADR Sense and CAT-1 will all be coupled with a weather station close to the span location to ensure the reliability of the measurements and to meet the N-1 criterion.

Incomes

The yearly cash flow is considered constant along the length of the analysis. It is calculated with the following formula:

$$CF_i = C_F - c_v E \qquad (23)$$

Where:

- **CF_i** is the total estimated yearly cash flow;
- **C_f** is the fixed cost the wind farm has to pay yearly to the DSO (Connection fee);
- **c_v** is the compensation the wind farm owner will receive from the DSO for the produced energy (based on the amount of losses that the facility causes or reduces);
- **E** is the yearly wind farm energy production.

The employed values (considered average values for Swedish grid owners) for the selected study case are reported in the following table:

Table 18: Incomes details.

C_f [SEK/year]	c_v [öre/kWh]	E [kWh/year]	CF_i [SEK/year]
595000	0.0024	75000000	**415000**

The resulting yearly cash flow is of 415 kSEK. It is considered the same for all the different solutions. This simplifying assumption is due to the impossibility to estimate at this stage the precise difference between the incomes for the considered options. All the uprating methods are considered suitable, and would not require energy curtailment from the wind farm, up to the installation of three different new wind farms (27 wind turbines).

Results

The results are obtained for different cases, taking in account different scenarios on the future wind turbines installation. Scenario 1 considers the case where only one wind farm will be installed in the whole analyzed period (20 years). The second scenario considers the installation of two wind farms at year one. The third considers the installation of three new wind farms at year 1. Lastly, scenario 4 considers the subsequent installation of a new wind farm each 3 years (one farm at year 1, another at year 4, the third and last at year 7). The results are below presented:

Table 19: Results for Scenario 1.

	Power Donut	CAT-1	ADR Sense	Cond. Substitution	New Line
NPV [MSEK]	3.61	2.22	4.12	-157.78	-130.06
DPP [Year]	2	4	1	-	-

Table 20: Results for Scenario 2.

	Power Donut	CAT-1	ADR Sense	Cond. Substitution	New Line
NPV [MSEK]	9.19	7.80	9.71	-152.19	-124.48
DPP [Year]	< 1	1	< 1	-	-

Table 21: Results for Scenario 3.

	Power Donut	CAT-1	ADR Sense	Cond. Substitution	New Line
NPV [MSEK]	14.77	13.38	15.29	-146.61	-118.90
DPP [Year]	< 1	1	< 1	-	-

Table 22: Results for Scenario 4.

	Power Donut	CAT-1	ADR Sense	Cond. Substitution	New Line
NPV [MSEK]	11.45	10.06	11.97	-149.93	-122.22
DPP [Year]	2	3	1	-	-

The results show that the DPP for the different DLR devices is short, even less than a year.

This should not surprise since the necessary equipment is relatively cheap in respect of the overall benefits received from the connection of a new wind farm. Similar results have been found for the installation of CAT-1 in [41].

The investments in the conductor upgrading and the construction of a new line show to have a negative impact for Ellevio AB in every scenario (negative NPV). This is due to the high investment costs that are needed for these operations. It should be considered that the possibility to upgrade the line with both, new conductors, and DLR equipment, would have a massive impact on the total transportable energy flow. For the selected case study it is not foreseen such an amount of new energy flowing in lines A and B to justify the relative investment levels.

Among the different DLR devices CAT-1 results to be the most expensive. It should be considered however that while CAT-1 monitor the average conditions of the entire 40 km line, PD and ADR sense would only report the condition of a single location of the weak span. Since line B location is characterized by different microclimates the installation of a single PD or ADR sense device can incur in problematic situations for the OHL. In order to compare CAT-1 with the other solutions precision, results are also obtained in the case that ADR sense and PD would be installed in four different locations, one each 10 kilometers. Results are reported in Table 23.

Table 23: Results obtained with the installation of four PD and ADR sense for scenario 1.

	Power Donut	CAT-1	ADR Sense
NPV [MSEK]	-2.32	2.22	-0.25
DPP [Year]	-	4	-

Results shows how in this last case PD and ADR sense would cause an economic loss for Ellevio AB (negative NPV). It is eventually concluded that CAT-1 is the suggested device to be applied to line B both from both a technical and economical points of view.

6. Conclusions and Future Works

The performed investigation proved that DLR is the best mean to introduce new wind farms in the network for the selected study-case. When the wind farm energy supply does not vary substantially the previous grid load, a dynamic monitoring of the OHLs ensures important ampacities improvements without the need of expensive grid upgrades, as the construction of a new line.

The monitoring of the lines is necessary to avoid annealing or clearance to ground issues caused by conductors overheating. The different climate data are analyzed in order to obtain the conductor temperature. This calculation can be performed using different conductor thermal models. To ensure a safe operation of the OHLs with a DLR approach it is necessary to certify the accuracy of the cited models and verify their effectiveness.

IEEE calculation standard has been analyzed and weaknesses have been found on the theoretical approach employed for the forced convective cooling calculation. Specifically the wind direction effect is estimated as the conductor is a perfect cylinder. A wind tunnel test have been performed in order to verify the effect of the conductor's strands on the total thermal equilibrium.

The results show that an inclined wind-conductor relative direction can have an higher impact on the line rating than foreseen with the IEEE 738 standard. Because of different laboratory deficiencies the obtained results have not been accurate enough to further investigate the precision level of the analyzed standard. The laboratory set-up precision and control should be improved in future projects in order to have a correct estimation of the conductor heat transients.

The test however confirmed the important influence that forced convective cooling has on the overall conductor thermal balance and proved that stranded conductors cannot be exactly compared with perfect cylinders.

The literature contains several investigation of the methods, both from a practical and a theoretical point of view. Theoretically different weakness in the methods are reported. Field-test experiences on the contrary show that the present precision level is accurate enough to utilize DLR on a larger scale. It is also true that, in Europe, the 15 TSOs that use DLR nowadays does not utilize it as an automatic answer to overload issues. This suggest that even if the employed devices are reliable, a wider field experience is needed to reach higher confidence level with the innovative technology.

Ellevio AB supplied the possibility to investigate the potential benefits of DLR on two weak OHLs in Värmland; a region located in the Southwest of Sweden.

The region has a high wind resource potential. For this reason wind farm owners want to increase the total wind power installed in the area. Specifically the work analyses the impact of the introduction of a 27 MW wind farm on a sensible grid. Two 130 kV OHLs are investigated and results show that, not only DLR would allow a full exploitation of the wind farm, but would also protect it from possible overheating contingencies due to SLR ampacities overestimations.

DLR is particularly suggested in the area because the same favorable wind conditions that power the wind turbines are capable of cooling down the OHL conductors allowing higher currents to be transferred.

If technically DLR proved its validity, economically it constitutes certainly the best choice for DSOs and TSOs which experience instances where the SLR would require energy curtailments in the pre-existing grid. Three different devices have been analyzed and results show that the investment necessary for the installation of conductors' monitoring equipment would be recovered rapidly in every different case. In a long run, the calculated NPV, shows how important can be the economical benefits that DSO would experience with the adoption of a dynamic line rating approach.

Bibliography

[1] S. P. Walldorf, S. John, and F. J. Hoppe, “The Use of Real-Time Monitoring and Dynamic Ratings for Power Delivery System and the Implications for Dielectric Materials,” *IEEE Electr. Insul. Mag.*, vol. 15, no. 5, 1999.

[2] M. Y. DAVIS, “A New Thermal Rating Aapproach: the Real Time Thermal Rating System for Strategic Overhead Conductor Transmission Lines. Part IV.,” *IEEE Trans. Power Appar. Syst.*, vol. PAS-99, no. 6, pp. 2184–2192, 1980.

[3] J. . Engelhardt and S. . Basu, “Design, Installation, and Field Experience with an Overhead Transmission Dynamic Line Rating System,” *IEEE*, 1996.

[4] P. Musilek, J. Heckenbergerova, and D. Koval, “Evaluating Thermal Aging Characteristics of Electric Power Transmission Lines,” *IEEE*, pp. 100–103, 2010.

[5] J. R. Harvey, “Effect of Elevated Temperature Operation on the Strength of Aluminum Conductors,” *IEEE Trans. Power Appar. Syst.*, vol. PAS-91, no. 5, p. 2007, 2007.

[6] D. O. Koval and B. Roy, “Determination of Transmission Line Ampacities by Probability and Numerical Methods,” *IEEE Trans. Power Appar. Syst.*, vol. PAS-89, no. 7, pp. 1485–1492, 1970.

[7] M. Piekutowski, T. L. Le, and M. Negnevitsky, “Expert System Application for the Loading Capability Assessment of Transmission Lines,” *IEEE Trans. Power Syst.*, vol. 10, no. 4, pp. 1805–1812, 1995.

[8] D. Committee, “IEEE Std 738-1993 IEEE Standard for Calculating the Current-Temperature Relationship of Bare Overhead Conductors.pdf,” *America*, vol. 1993. 1993.

[9] F. I. Oluwajobi, O. S. Ale, A. Ariyanninuola, and C. A. O. F. I, “Effect of Sag on Transmission Line,” vol. 3, no. 4, pp. 627–630, 2012.

[10] E. Lindberg and E. Lindberg, “The Overhead Line Sag Dependence on Weather Parameters and Line Current current,” no. December, 2011.

[11] IEEE, “IEEE SA - C2-1990 - National Electric Safety Code,” 1990.

[12] Elsäkerhetsverkets, “ELSÄK-FS 2008:1,” 2008.

[13] CIGRÉ WG 22.12, “The thermal behaviour of overhead conductors,” *Electra*, no. 144, 1992.

[14] N. P. Schmidt, S. Member, and A. H. B. Equalion, “Comparison Between IEEE and CIGRE Ampacity Standards,” vol. 14, no. 4, pp. 1555–1562, 1999.

[15] L. Staszewski and W. Rebizant, “The Differences between IEEE and CIGRE Heat Balance Concepts for Line Ampacity Considerations,” 2010.

[16] W. McAdams, “Heat Transmission,” in *Heat Transmission*, 1954, pp. 165–183.

[17] D. A. Douglass and A. Edris, “Field Studies of Dynamic Thermal Rating Methods For Overhead Lines,” pp. 842–851, 1999.

[18] D. A. Douglass, D. C. Lawry, A. Edrisz, and E. C. Bascom, “Dynamic Thermal Ratings

Realize Circuit Load Limits," 1992.

[19] R. Mai, L. Fu, and Xu HaiBo, "Dynamic line rating estimator with synchronized phasor measurement," in *APAP 2011 - Proceedings: 2011 International Conference on Advanced Power System Automation and Protection*, 2011, vol. 2, pp. 940–945.

[20] S. S. Mousavi-Seyedi, F. Aminifar, S. Azimi, and Z. Garoosi, "On-line assessment of transmission line thermal rating using PMU data," in *Smart Grid Conference 2014, SGC 2014*, 2014.

[21] J. Fu, D. J. Morrow, and s. abdelkader, "Integration of Wind Power into Existing Transmission Network by Dynamic Overhead Line Rating." 2012.

[22] J. Fu, S. Abbott, B. Fox, D. J. Morrow, and S. Abdelkader, "Wind cooling effect on dynamic overhead line ratings," in *Universities Power Engineering Conference (UPEC)*, 2010.

[23] S. Islam and F. Islam, "Impact of Temperature, Wind Flow, Solar Radiation, Skin Effect and Proximity Effect on Overhead Conductor," vol. 12, no. 1, 2012.

[24] S. Talpur, C. J. Wallnerstrom, P. Hilber, and C. Flood, "Implementation of Dynamic Line Rating in a Sub-Transmission System for Wind Power Integration. Smart Grid and Renewable Energy Implementation of Dynamic Line Rating in a Sub-Transmission System for Wind Power Integration," *Smart Grid Renew. Energy*, vol. 6, no. 6, pp. 233–249, 2015.

[25] M. W. Davis, "A New Thermal Rating Aapproach: the Real Time Thermal Rating System for Strategic Overhead Conductor Transmission Lines. Part II.," *IEEE Transic. Power Appar. Syst.*, vol. PAS-96, pp. 18–23.

[26] A. Ghanem, C. Habchi, T. Lemenand, D. Della Valle, and H. Peerhossaini, "Energy efficiency in process industry - High-efficiency vortex (HEV) multifunctional heat exchanger," *Renew. Energy*, vol. 56, pp. 96–104, 2013.

[27] K. A. Thole, R. W. Radomsky, M. B. Kang, and A. Kohli, "Elevated freestream turbulence effects on heat transfer for a gas turbine vane," *Int. J. Heat Fluid Flow*, vol. 23, no. 2, pp. 137–147, 2002.

[28] S. Foss, S. Lin, H. Stillwell, and R. Fernandes, "Dynamic Thermal Line Ratings Part II Conductor Temperature Sensor and Laboratory Field test Evaluation," *IEEE Trans. Power Appar. Syst.*, vol. PAS-102, no. 6, pp. 1865–1876, Jun. 1983.

[29] S. D. Foss, S. H. Lin, and R. Carberry, "Significance of the Conductor Radial Temperature Gradient within a Dynamic Line Rating Methodology," *IEEE Transactions on Power Delivery*, vol. 2, no. 2. pp. 502–511, 1987.

[30] B.Clairmont, D.A.Douglass, J.Iglesias, and Z.Peter, "Radial and longitudinal temperature gradients in bare stranded conductors with high current densities," *CIGRE*, vol. B2, no. 108, 2012.

[31] S. H. Lin, "Heat transfer in an overhead electrical conductor," vol. 35, 1992.

[32] "USB TC-08 Specifications." [Online]. Available: https://www.picotech.com/data-logger/tc-08/usb-tc-08-specifications.

[33] "lab-VIEW." [Online]. Available: http://www.ni.com/labview/.

[34] I. Makhkamova, P. C. Taylor, J. R. Bumby, and K. Mahkamov, "CFD analysis of the

thermal state of an overhead line conductor," in *Proceedings of the Universities Power Engineering Conference*, 2008.

[35] K. M. Klein, P. L. Springer, and W. Z. Black, "Real-time ampacity and ground clearance software for integration into smart grid technology," *IEEE Trans. Power Deliv.*, vol. 25, no. 3, pp. 1768–1777, 2010.

[36] S. H. Lin and S. D. Foss, "Significance Of The Conductor Radial Temperature Gradient Within a Dynamic Line Rating Methodology," *IEEE Trans. Power Deliv.*, vol. PWRD-2, no. 2, pp. 502–511, 1987.

[37] S. P. Warren Wang, "Dynamic Line Rating Systems for Transmission Lines," 2014.

[38] E. Fernandez, I. Albizu, M. T. Bedialauneta, A. J. Mazon, and P. T. Leite, "Dynamic line rating systems for wind power integration," in *IEEE Power and Energy Society Conference and Exposition in Africa: Intelligent Grid Integration of Renewable Energy Resources (PowerAfrica)*, 2012, pp. 1–7.

[39] E. M. Carlini, F. Massaro, and C. Quaciari, "Methodologies to uprate an overhead line. Italian TSO case study," *J. Electr. Syst.*, vol. 9, no. 4, pp. 422–439, 2013.

[40] J. Ausen, B. Fitzgerald, E. Gust, D. Lawry, J. Lazar, and R. Oye, "Dynamic Thermal Rating System Relieves Transmission Constraint," in *ESMO 2006 - 2006 IEEE 11th International Conference on Transmission & Distribution Construction, Operation and Live-Line Maintenance*, 2006.

[41] "CAT-1." [Online]. Available: http://www.nexans.com/eservice/Navigate.nx?CZ=Corporate&language=en&navigationId=318444.

[42] "ADR SENSE." [Online]. Available: http://www.ampacimon.com/adr-sense/.

[43] B. Forbes, D. Bradshaw, and F. Campbell, "Finding Hidden Capacity In Transmission Lines," *Transm. World*, 2002.

[44] "Spansentry." [Online]. Available: http://avistarinc.com/images/documents/span-sentry/SpanSentry-product-sheet-Jan2014web.pdf.

[45] "Promethean Devices™ Real-Time Monitoring Solution for Transmission Lines." [Online]. Available: http://www.stabiloy.com/nr/rdonlyres/ab0f9631-240d-46f2-a755-3afcb807eacb/0/prometheandevicesdatasheetut0007a.pdf. [Accessed: 19-May-2016].

[46] J. K. Raniga and R. K. Rayudu, "Dynamic rating of transmission lines-a New Zealand experience," in *2000 IEEE Power Engineering Society Winter Meeting. Conference Proceedings (Cat. No.00CH37077)*, 2000, vol. 4, pp. 2403–2409.

[47] U. Power, "PD3™ (Power Donut) Line Monitor Overview." [Online]. Available: http://www.usi-power.com/Products & Services/Donut/Overview/Overview.htm.

[48] Usi, "Power Donut2 ™ The Instrumentation Platform For High Voltage Power Systems." 2009.

[49] Arteche, "SMT." [Online]. Available: http://arteche.com/es/ficha-t%C3%A9cnica-smt.

[50] MICCA, "EMO, Easy monitoring overhead transmission." [Online]. Available: http://www.ohtlgrid.com/en/ueberemo/ueberemo.html.

[51] ENTSOE, “Dynamic Line Rating for overhead CE TSOs current practice,” 2015.

[52] I. Albizu, A. J. Mazón, and I. Zamora, “Methods for Increasing the Rating of Overhead Lines,” pp. 1–6.

[53] F. Kiessling, D. Hussels, C. Juerdens, and J. Ruhnau, “Upgrading high-voltage lines to increase their capacity and mitigate environmental impacts,” *CIGRE Sess.*, vol. 22, no. 208, 1998.

[54] Broschat and Myron, “Transmission Line Uprating 115kV to 230 kV Report on Operating Performance,” *IEEE Trans. Power Appar. Syst.*, vol. PAS-91, no. 2, pp. 545–548, Mar. 1972.

[55] J. G. Hanson, “Upgrading Transmission Lines,” *Transm. Distrib. Conf.*, pp. 824–827, 1991.

[56] D. Sanchez and C. Alonso, “Increase in transmission capacity in highvoltage power lines on the Levante (Eastern Spain) coastal path,” *CIGRÉ Sess.*, vol. V2, no. 206, 2004.

[57] R. Stephen and D. Muftic, “Determination of the thermal rating and uprating methods for existing lines,” *CIGRÉ Sess.*, vol. 2004, no. V2, p. 317.

[58] S. P. Hoffmann and A. M. Clark, “The approach to thermal uprating of transmission lines in the UK,” *CiIGRE Sess.*, vol. 22, no. 305, 2004.

[59] C. Q. E.M. Carlini, S Favuzza, S.E. Giangreco, F. Massaro, “Uprating an Overhead Line. Italian TSO Applications to Increase System N-1 Security.,” 2013, no. October, pp. 20–23.

[60] M. J. Tunstall, S. P. Hoffmann, N. S. Derbyshire, and M. J. Pyke, “Maximising the ratings of National Grid’s existing transmission lines using high temperature low sag conductor,” *”, CIGRÉ Sess.*, vol. 22, no. 202, 2000.

[61] I. Zamora, A. J. Mazón, P. Eguía, R. Criado, C. Alonso, J. Iglesias, and J. R. Saenz, “High-temperature conductors: A solution in the uprating of overhead transmission lines,” in *2001 IEEE Porto Power Tech Proceedings*, 2001, vol. 4, pp. 61–66.

[62] F. R. Thrash, “ACSS/TW-an improved conductor for upgrading existing lines or new construction,” in *1999 IEEE Transmission and Distribution Conference (Cat. No. 99CH36333)*, 1999, vol. 2, pp. 852–857 vol.2.

[63] R. C. Gupta, *Energy and Environmental Management in Metallurgical Industries*. New Delhi, 2012.

[64] Svensk Vindenergy, “Vindkraftstatistik och prognos, Kvartal 4 2015,” 2016.

[65] A. M. Held, “Modelling the future development of renewable energy technologies in the European electricity sector using agent-based simulation,” Karlsruher Instituts für Technologie (KIT), 2010.

[66] “Rabbalshedekraft.” [Online]. Available: http://www.rabbalshedekraft.se/Vindparker/.

[67] Google, “Google Maps.” [Online]. Available: https://maps.google.com/.

[68] “NASA Surface meteorology and Solar Energy.” [Online]. Available: https://eosweb.larc.nasa.gov/cgi-bin/sse/grid.cgi?&num=193150&lat=59.25&submit=Submit&hgt=100&veg=17&sitelev=&email=skip@larc.nasa.gov&p=grid_id&p=wnd_dir&step=2&lon=12.11.

[69] M. Ragheb, “Wind Shear, Roghness Classes and Wind Energy Production,” 2015.

[70] Swedish University of Agricultural Sciences, “Arvika weather data.” [Online]. Available: http://www.slu.se/sv/fakulteter/nj/om-fakulteten/ovriga-enheter/faltforsk/vader/].

[71] N. Di Franco, “Introduzione All’analisi Economica Degli Investimenti,” 2007.

[72] Sverige Riksbank, “Current forecast for the repo rate, inflation and GDP,” 2016. [Online]. Available: http://www.riksbank.se/en/Monetary-policy/Forecasts-and-interest-rate-decisions/Current-forecast-for-the-repo-rate-inflation-and-GDP/.

[73] S. D. Foss, S. H. Lin, and H. R. Stillwell, “Dynamic Thermal Line Ratings Part II, Conductor Temperature Ssensor and Laboratory Field Test Evaluation 1865,” no. 6, 1983.

Appendix A Excel and Matlab model inputs.

The parameters are listed in the following table:

Conductor characteristics	
Name	Ibis
Type	ACSR
N°aluminium/n°steal strands	26/7
Area	234 mm^2
Resistance	0.1434 Ω/km
Specific heat	0.534 j/g°C
Weight	813 Kg/Km
Emissivity ε	0.8
Absorptivity α	0.8

Wind Turbine	
Model	Vestas 112
Nominal power	3.075 MW
Number of Turbines	9
Hub height	119 m
Swept Area	9.852 m^2
Cut-in Wind speed	3 m/s
Rated Wind speed	13 m/s
Cut-out Wind speed	25 m/s

Span Characteristic	
Direction	77°
Height	6.4 m

Location	
Latitude	59.51 ° North
Height OSL	200 m

In addition to the cited parameters the following data are used to run the simulation:

- **Weather data**

The SMHI weather station of Arvika is depicted in the following picture.

Figure 1: SMHI weather station in Arvika. Picture of July 2015 [1].

[1] http://www.smhi.se/bloggar/vaderleken/2015/07

Air temperature, wind speed and direction are recorded with a 3 hours interval resolution.

The weather station installation follows the guidelines of the World Meteorological Organization [WMO] [2]. Thus, the wind is measured at 10 meters height.

The station is located 17 km far from the selected hot.

- **Load data**

  The active power flow data are available from ELLEVIO AB database for both line A and B. The current flowing on each conductor is obtained through:

$$I = \frac{P}{V * \sqrt{3}}$$

Where V is 130 kV.

- **The Wind power** supply is calculated from the wind data at hub height in Årjäng.

Calculation

The calculation follows the IEEE model. Joule and solar heating, and Convective and radiative cooling are considered.

Only one calculation procedure is different in respect of the IEEE standard. Since resistances values are available only for 20 °C temperature in supplier catalogues; CIGRE approach is used to correct the resistance value at different conductor temperatures. [3]

$$R_T = R_{20°C}[1+\propto (T-20)]$$

Where $\propto$ = 0.0036 as cited in the CIGRE standard for ACSR [3].

[2] http://www.wmo.int/pages/prog/www/IMOP/publications/CIMO-Guide/Ed2008Up2010/Part-I/WMO8_Ed2008_PartI_Ch5_Up2010_en.pdf

[3] CIGRÉ WG 22.12, "The thermal behaviour of overhead conductors," *Electra*, no. 144, 1992.

Appendix B: Matlab script. Solar heat flux calculation.

```
clc
clear all

%%Solar heat flux calculation

%input reading

filename = 'Steady-state year.xlsx';
sheet = 'Sheet1';
xlRange = 'D2:D2921';
OM= xlsread(filename,sheet,xlRange);        %Hour angle relative to noon,
15*(Time-12), at 11AM,Time = 11 and the Hour angle= -15 [deg]

filename = 'Steady-state year.xlsx';
sheet = 'Sheet1';
xlRange = 'A2:A2921';
N= xlsread(filename,sheet,xlRange);         %Day of the year (January 21 = 21,
Solstices on 172 and 355)

Lat=59.508376;                              %Latitude [deg]

sig=23.46*sind(((284+N)/365)*360);          %Solar declination angle [deg]




for i=1:2920

    Hc(i)=asind(cosd(Lat)*cosd(sig(i))*cosd(OM(i))+sind(Lat)*sind(sig(i)));
%Altitude of the sun deg

    X(i)=(sind(OM(i))/(sind(Lat)*cosd(OM(i))-cosd(Lat)*tand(sig(i))));
%Solar Azimuth variable

    if X(i) < 0
        if OM(i)<0
            C(i)=180;                       %Solar Azimuth constant [deg]

        else
            C(i)=360;
        end


    else

        if OM(i)<0
            C(i)=0;

        else
            C(i)=180;
        end
    end
end
```

```
Zc=C'+atand(X');                              %Azimuth of the sun deg



% heat flux equation parameters input

A1=-42.2391;
B1=63.8044;
C1=-1.9220;
D1=3.46921e-2;
E1=-3.61118e-4;
F1=1.94318e-6;
G1=-4.07608e-9;


Qss=A1+B1*Hc+C1*Hc.^2+D1*Hc.^3+E1*Hc.^4+F1*Hc.^5+G1*Hc.^6;      %total heat
flux sea level w/m2

%Altitude correction factor

He=200;                     %Altitude of conductor m
B2=1.148e-4;
C2=-1.108e-8;
Kse=1+B2*He+C2*He.^2;
Qse=Kse*Qss;                %total heat flux at Altitude He;


%result writing

filename = 'Steady-state year.xlsx';
sheet = 'Sheet1';
Ap= xlsread(filename,sheet,'AK2');    %Projected area of conductor m2/m


Zl=77;                                %line direction East west=77°
for i=1:2920
    theta(i)=acosd(cosd(Hc(i))*cosd(Zc(i)-Zl));         %effective incident
angle
    alpha=0.8;                                          %Solar absorptivity
    qs(i)=alpha*Qse(i)*sind(theta(i))*Ap;               %solar heat rate [W/m]
    if qs(i)<0
        qs(i)=0;
    end

end


%conductor wind relative angle calculation

%direction (360 deg) reading

xlRange = 'Z2:Z2921';
sheet='Sheet1';
xlswrite('Steady-state year.xlsx', {'qs [W/m]'} , sheet, 'Z1');
xlswrite('Steady-state year.xlsx', qs', sheet,xlRange);
```

```
filename = 'Steady-state year.xlsx';
sheet = 'Sheet1';
xlRange = 'G2:G2921';
DIR= xlsread(filename,sheet,xlRange);

for i=1:2920;

    if   DIR(i) <77
        DIRR(i)=77-DIR(i);

    elseif DIR(i) <=167
        DIRR(i)=DIR(i)-77;
    elseif DIR(i) <=257
        DIRR(i)=257-DIR(i);
    elseif DIR(i) <=347
        DIRR(i)=DIR(i)-257;
    else
        DIRR(i)=DIR(i)-360+77;
    end

end

    %results writing

    xlRange = 'H2:H2921';
    sheet='Sheet1';

    xlswrite('Steady-state year.xlsx', DIRR', sheet,xlRange);
```